Energy Engineering

Tech Science Press

http://doi.org/10.32604/ee.2026.074212

ARTICLE

Research on Intelligent Network Formation and Flexible Interconnection Mechanisms for Low-Voltage Distribution Networks in Cyber-Physical Systems

Xieli Fu, Guoxing Wu*, Yujie Shi, Xinming Jiang and Wenfeng Yang

Shenzhen Power Supply Bureau Co., Ltd., Power Grid Planning Research Center, Shenzhen, China
*Corresponding Author: Guoxing Wu. Email: guoxingwu2025@163.com

Received: 05 October 2025; Accepted: 04 March 2026; Published: 24 September 2026

ABSTRACT: Low-voltage distribution networks face critical challenges from large-scale distributed renewable energy integration, including bidirectional power flow control, voltage stability, and multi-microgrid coordination. Existing approaches are limited by single-scenario optimization without cyber-physical coupling considerations, device-level control lacking system-level coordination, and absence of unified frameworks bridging topology reconfiguration with power exchange. This study proposes a collaborative framework integrating intelligent network formation and flexible interconnection within a cyber-physical system environment. A four-layer architecture featuring edge-cloud collaborative computing and fault-tolerant hybrid communication was constructed. A multi-agent coordination algorithm based on TD3 deep reinforcement learning was developed for distributed decision-making with consensus-guaranteed convergence. A flexible interconnection control strategy based on virtual synchronous generator technology was designed for multi-microgrid power exchange with inherent inertia support. Validation was conducted through offline simulation (IEEE 33/69-node systems), hardware-in-the-loop testing (OPAL-RT ePHASORSIM), and field deployment across residential (150 households, 450 kW PV), industrial (5 MW peak load, 2 MWh storage), and commercial (3 MW peak demand) scenarios in Shenzhen. The multi-agent algorithm achieved over 60% faster convergence than conventional metaheuristics, with a load balancing index of 0.098 and computation time of 52 s. The flexible interconnection strategy reduced voltage regulation time by 73% (from 12 s to 3.2 s) and frequency deviation by 81% (from ±0.8 Hz to ±0.15 Hz). System performance reached 99.97% power supply reliability, 91.2% energy efficiency, 41% network loss reduction, and 21% annual operating cost reduction with 6.5–8.5 year payback periods. This framework provides a validated technical solution for intelligent upgrading of low-voltage distribution networks under high renewable penetration.

KEYWORDS: Deep reinforcement learning; virtual synchronous generator; cyber-physical system; low-voltage distribution networks; multi-agent coordination

1 Introduction

The modern power system, driven by the energy transition, is undergoing a profound transformation from traditional centralized architectures to distributed smart grids. As the critical link connecting transmission systems to end users, low-voltage distribution networks face unprecedented challenges such as large-scale integration of distributed renewable energy, bidirectional power flow control, and power quality assurance [1]. The integration of cyber-physical system (CPS) technologies offers new technical pathways to address these challenges. By deeply integrating computational, communication, and physical control processes, CPS enables intelligent perception, decision-making, and control within distribution networks [2]. The application of artificial intelligence (AI) technologies in power systems is reshaping traditional operational models, demonstrating immense transformative potential particularly in system optimization, predictive analytics, and adaptive control [3].

Existing research on cyber-physical systems for power grids can be categorized into three main streams, each with distinct limitations that motivate the present study:

First, AI-driven optimization approaches have made substantial progress in intelligent network formation. Smart grid formation, as a core technology for next-generation distribution networks, enables dynamic reconfiguration and optimal configuration of network topology through machine learning algorithms and optimization theory [4]. The application of distributed artificial intelligence in distribution system planning and operation continues to deepen, providing effective means to address system complexity, uncertainty, and multi-objective optimization problems [5]. The use of distributed machine learning methods, such as federated learning, in smart grids opens new avenues for collaborative decision-making while protecting data privacy [6]. However, these approaches primarily optimize single operational scenarios without accounting for the deep coupling characteristics between cyber and physical layers. Existing algorithms typically assume ideal communication conditions and do not consider network delays, packet loss, or information security threats inherent in cyber-physical environments. Furthermore, most studies focus on transmission-level systems, with insufficient attention to the unique characteristics of low-voltage distribution networks, such as high R/X ratios, unbalanced three-phase loads, and high renewable penetration.

Second, decentralized control architectures and flexible interconnection technologies have emerged as key enablers for microgrid coordination. Flexible interconnection technologies, through advanced control strategies and energy storage system integration, enable microgrids to maintain stability and reliability under various operating conditions [7]. As a key vehicle for achieving 100% renewable energy targets, microgrids have seen increasingly mature research in modeling methods and energy management strategies, encompassing critical technologies such as multi-timescale optimization, uncertainty modeling, and system resilience enhancement [8]. The application of decentralized control architectures in microgrid systems is driving a transformation in traditional grid management paradigms [9,10]. Distribution network reconfiguration technologies leverage intelligent algorithms for topological optimization, playing a vital role in enhancing system operational efficiency and strengthening network resilience [11]. Nevertheless, current flexible interconnection mechanisms are largely confined to device-level control strategies, such as droop control and voltage regulation at the point of common coupling. System-level coordination mechanisms that enable multi-microgrid cooperative operation remain insufficiently explored. Technical challenges persist in control coordination, information exchange, and fault handling under real-world communication constraints. Moreover, existing decentralized approaches often lack effective global optimization frameworks, leading to suboptimal performance when managing large-scale interconnected systems.

Third, cyber-physical system integration for power applications has received growing attention. Deep learning-driven distributed cyber-physical systems provide technological support for intelligent management of renewable energy communities [12]. Research has progressed in areas such as biomimetic intelligent control [13], decentralized energy management [14], and artificial intelligence applications [15]. While existing CPS architectures have established foundational frameworks integrating information and physical layers, they exhibit three critical limitations when applied to low-voltage distribution networks: (1) Generality over specificity: These architectures are designed for broad power system applications without tailored optimization for low-voltage network characteristics, such as high impedance ratios, voltage sensitivity, and rapid load fluctuations. (2) Vertical integration without horizontal coordination: Current architectures emphasize hierarchical information flow (sensors $\rightarrow$ cloud $\rightarrow$ control) but lack mechanisms for peer-to-peer coordination among distributed agents, limiting real-time responsiveness and scalability. (3) Separation of grid formation and flexible interconnection: Intelligent grid topology optimization and microgrid interconnection control are treated as independent functional modules without unified coordination frameworks, preventing holistic system optimization.

These three research streams—AI optimization, decentralized control, and CPS integration—have advanced their respective domains but remain inadequately integrated. Critical technological gaps persist in several key areas: intelligent network formation algorithms lack universal frameworks that account for cyber-physical coupling characteristics; flexible interconnection mechanisms require system-level coordination beyond device control; and unified optimization theories bridging grid formation and flexible interconnection are absent. The transition from isolated optimization to integrated coordination, from device-level control to system-level orchestration, and from single-scenario solutions to adaptive multi-scenario frameworks remains a significant challenge.

To address these identified gaps, this study aims to achieve three primary research objectives:

(1) Architecture Design Objective: Develop a layered cyber-physical system architecture specifically tailored for low-voltage distribution networks, featuring: (a) edge-cloud collaborative computing to balance real-time local control with global optimization; (b) redundant communication pathways to ensure fault tolerance under network disruptions; and (c) standardized interfaces enabling plug-and-play integration of heterogeneous devices from multiple vendors.

(2) Algorithm Development Objective: Design a multi-agent coordination algorithm that unifies local intelligence with global optimization through: (a) deep reinforcement learning-based distributed decision-making, where each agent learns optimal policies through environmental interaction; (b) consensus protocols ensuring convergence despite communication delays and topology changes; and (c) robust optimization mechanisms addressing renewable energy uncertainty and load variability.

(3) System Integration and Validation Objective: Validate the proposed framework through comprehensive testing encompassing: (a) pure software simulation using IEEE 33/69-node test systems; (b) hardware-in-the-loop co-simulation integrating real controllers with OPAL-RT real-time simulators; and (c) field deployment across three typical scenarios (residential areas, industrial parks, commercial districts) with varying renewable penetration (15–45%) and load characteristics.

The expected research outcomes include: Enhanced system response speed (>70% improvement in voltage/frequency regulation time), superior stability margins (>100% increase in damping ratio and voltage stability), significant economic benefits (>20% reduction in operating costs), and comprehensive validation demonstrating practical deployability in real-world distribution networks.

The novelty of this work lies in three key contributions that distinguish it from existing research:

(1) A unified cyber-physical system architecture for low-voltage distribution networks. Unlike existing CPS architectures designed for transmission-level systems or general power applications, the proposed four-layer architecture (physical device, network communication, data processing, application service) is specifically optimized for low-voltage network characteristics. Key innovations include: (a) Edge intelligence: Distributing computation to network edges reduces communication overhead and enables millisecond-level local responses critical for voltage stability in low-voltage systems. (b) Adaptive communication: Hybrid wired-wireless protocols dynamically adjust bandwidth allocation based on network congestion and priority, ensuring quality-of-service for time-critical control signals. (c) Cyber-physical co-design: Simultaneous optimization of physical topology (switch configurations) and information topology (agent communication networks) achieves superior performance compared to sequential design approaches.

(2) The first integration of deep reinforcement learning-based multi-agent coordination with virtual synchronous generator technology. While multi-agent systems have been applied to power system optimization [16], and virtual synchronous generators have been used for microgrid control through reinforcement-learning-based parameter tuning [17] and fuzzy adaptive control [18], their combination for unified grid formation and flexible interconnection represents a novel contribution. This integration achieves: (a) Rapid convergence: Deep reinforcement learning enables agents to learn near-optimal policies through simulated experiences before deployment, reducing online optimization time by >60% compared to traditional metaheuristics. (b) Stability enhancement: Virtual synchronous generator control provides inherent inertia and damping, complementing the multi-agent system's fast response with smooth transient behavior. (c) Scalability: The distributed architecture naturally scales to hundreds of nodes without exponential computational growth, unlike centralized optimization methods.

(3) Comprehensive validation spanning pure simulation, hardware-in-the-loop, and real-world deployment. Most existing studies validate algorithms through software simulation alone or limited hardware experiments [19]. This work provides end-to-end validation demonstrating: (a) algorithmic correctness through MATLAB/Simulink modeling; (b) real-time feasibility through OPAL-RT hardware-in-the-loop testing with actual communication delays and computational constraints; and (c) engineering practicality through pilot deployment in three operational distribution networks serving >500 users, proving robustness under real-world uncertainties such as weather variability, equipment failures, and cyber disturbances.

Methodological Framework: This research adopts a cyber-physical co-simulation framework validated through multi-level testing. The study employs OPAL-RT ePHASORSIM real-time simulators for electromagnetic/electromechanical transient modeling, ns-3 network simulator for communication system emulation, and MATLAB/Simulink for algorithm development. The validation methodology progresses through three stages: (1) offline simulation establishing baseline performance with IEEE standard test systems under controlled conditions; (2) hardware-in-the-loop simulation integrating physical controllers, communication devices, and protection relays to verify software-hardware compatibility; and (3) field pilot testing in operational networks in Shenzhen, China, encompassing residential areas (150 households, 450 kW rooftop PV), industrial parks (5 MW peak load, 2 MWh battery storage), and commercial districts (3 MW peak load, demand response-enabled buildings). Performance metrics evaluated include convergence speed, voltage/frequency stability, energy efficiency, power supply reliability, and economic viability across normal operation, fault conditions, and extreme scenarios.

This research holds significant theoretical value and practical implications for enhancing distribution system operational efficiency, strengthening network self-healing capabilities, and ensuring power supply reliability. By providing a complete theoretical foundation and technical solution for the intelligent upgrading of low-voltage distribution networks, this work plays a positive role in advancing smart grid technology and constructing new power systems. For building energy systems specifically, the proposed technologies enable: (1) coordinated control of rooftop photovoltaic systems and battery storage at the building level; (2) seamless integration of demand response mechanisms with HVAC, lighting, and appliance loads; (3) building-to-grid services through flexible interconnection, allowing buildings to provide ancillary services such as voltage support and frequency regulation while optimizing their own energy costs. These capabilities enhance both individual building energy efficiency and overall grid stability, contributing to sustainable urban energy infrastructure development. Furthermore, the framework supports broader energy transition goals, including carbon peak and carbon neutrality objectives, by facilitating high renewable energy penetration while maintaining grid stability and economic viability.

2 Materials and Methods

2.1 Design of Cyber-Physical System Architecture for Low-Voltage Distribution Networks

The cyber-physical system architecture provides a unified design framework for the intelligent transformation of low-voltage distribution grids. By deeply integrating physical power systems with information and communication technologies, it enables comprehensive perception, intelligent decision-making, and coordinated control of distribution grids. The proposed low-voltage distribution grid cyber-physical system architecture adopts a layered design approach, establishing four core layers: the physical device layer, network communication layer, data processing layer, and application service layer, as shown in Fig. 1.

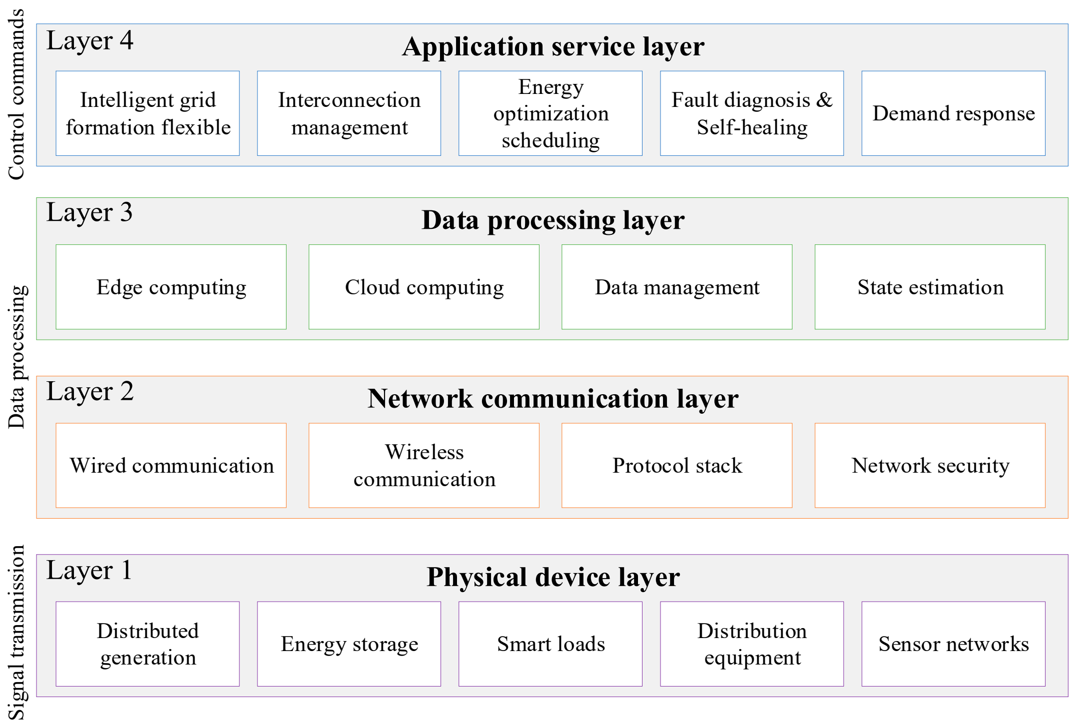

Figure 1: Cyber-physical system architecture for low-voltage distribution networks.

The Physical Device Layer, serving as the foundational layer, incorporates key components such as distributed generation units, energy storage systems, smart loads, distribution equipment, and sensor networks. Distributed generation units primarily include renewable energy devices like photovoltaic and wind power generation. Energy storage systems provide power balancing and power quality support. Smart loads enable active load regulation through demand response technologies. Distribution equipment handles power transmission and transformation functions. Sensor networks are responsible for real-time collection of system operational status information.

The network communication layer ensures reliable data transmission for the cyber-physical system, employing a hybrid communication architecture combining wired and wireless technologies. Wired communication includes fiber optic and power line carrier communication, while wireless communication encompasses technologies like WiFi, 5G, and LoRa. The communication protocol layer utilizes power system standards such as IEC 61850 and Modbus to guarantee system interoperability.

The data processing layer establishes a collaborative architecture integrating edge computing and cloud computing. Edge computing nodes handle real-time data preprocessing and local decision-making, while the cloud computing platform provides big data analytics and machine learning support. The data management system enables standardized data storage and secure access, with the state estimation module achieving accurate perception of distribution network operational status through multi-source data fusion technology.

The application service layer delivers user-oriented intelligent applications and services, including core functional modules such as smart grid configuration control, flexible interconnection management, energy optimization dispatch, fault diagnosis, and self-healing. Through coordinated operation, these modules achieve intelligent operation and optimized control of the distribution network.

Fig. 1 achieves deep integration of information flow and energy flow through hierarchical design, with bidirectional interaction between layers via standardized interfaces. Real-time data from the physical device layer is uploaded through the network communication layer to the data processing layer for analysis. The application service layer generates control strategies based on processing results and issues them for execution. This collaborative mechanism provides unified platform support for intelligent network formation and flexible interconnection in low-voltage distribution grids, ensuring system real-time performance, reliability, and intelligence.

2.2 Development of Intelligent Network Formation Algorithms and Mechanisms

The intelligent network restructuring algorithm is the core technology enabling adaptive reconfiguration and optimized operation of low-voltage distribution networks. By employing multi-agent coordination mechanisms and distributed optimization algorithms, it achieves dynamic adjustment of distribution network topology and optimal resource allocation. This study developed a comprehensive algorithmic framework encompassing four key components: network state sensing, topology optimization decision-making, multi-agent coordination, and dynamic restructuring execution.

2.2.1 Algorithmic Framework and Module Interaction

The intelligent network formation algorithm operates through a hierarchical four-stage workflow with clearly defined data flows and communication protocols, as illustrated in Fig. 2.

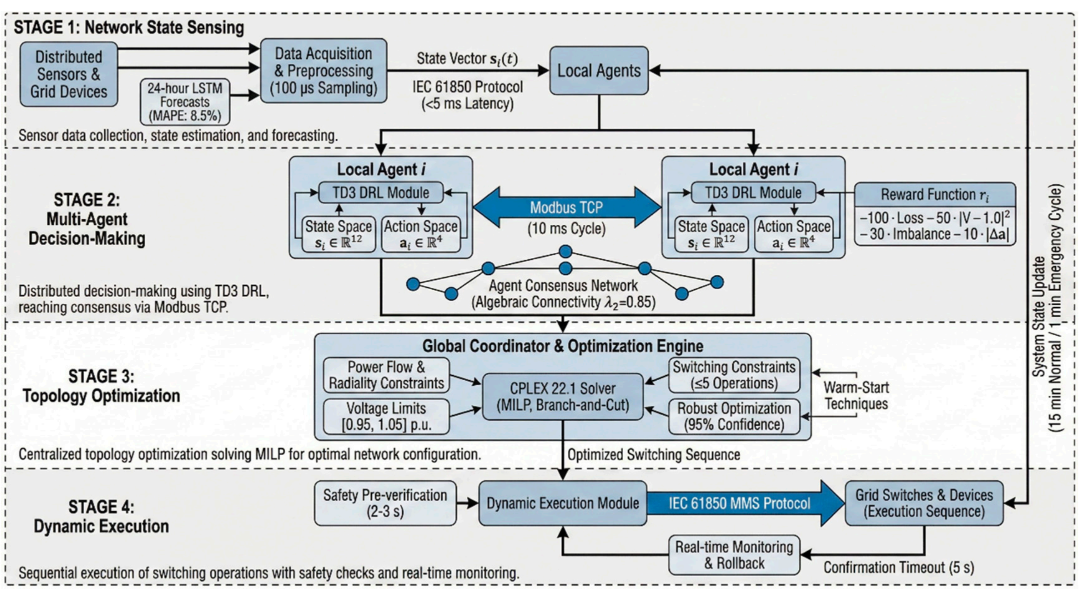

Figure 2: Hierarchical four-stage intelligent network formation algorithm workflow.

Stage 1—Network State Sensing: Distributed sensors collect real-time measurements (voltage, current, power, frequency) at 100 μs sampling intervals, constructing state vector $\mathbf{s}_i(t) = [V_i, f_i, P_i, Q_i, \mathrm{SOC}_i]^T$ for each node. Combined with 24-h LSTM forecasts (MAPE: 8.5%), validated states are transmitted to local agents via IEC 61850 protocol with <5 ms latency.

Stage 2—Multi-Agent Decision-Making: Each agent implements Twin Delayed Deep Deterministic Policy Gradient (TD3) algorithm with state space $\mathbf{s}_i \in \mathbb{R}^{12}$ (local measurements, neighbor states, historical trends, forecasts) and continuous action space $\mathbf{a}_i \in \mathbb{R}^4$ (DG/ESS power adjustments). The reward function balances four objectives: $r_i = -100 \cdot \mathrm{Loss} - 50 \cdot |V - 1.0|^2 - 30 \cdot \mathrm{Imbalance} - 10 \cdot |\Delta \mathbf{a}|$. Neural networks (architecture: 12-256-256-128-4) are trained with learning rates 10^{-4} (actor) and 10^{-3} (critic), batch size 256, and replay buffer 10^6. Convergence is ensured through: (1) communication topology with algebraic connectivity $\lambda_2 = 0.85$, (2) consensus protocol $\pi_i^{(k+1)} = 0.7\pi_i^{(k)} + 0.3\sum_{j\in\mathcal{N}_i} w_{ij}\pi_j^{(k)}$, and (3) Lyapunov stability guarantees. Agents exchange decisions via Modbus TCP (10 ms cycle) to reach consensus.

Stage 3—Topology Optimization: The global coordinator aggregates agent decisions and solves a mixed-integer linear programming problem minimizing network losses, switching costs, and voltage deviations subject to power flow, radiality, voltage limits [0.95, 1.05] p.u., and switching constraints (≤5 operations). CPLEX 22.1 solver with branch-and-cut algorithm provides solutions in 12–18 s using warm-start techniques. Chance-constrained optimization with 95% confidence bounds addresses renewable energy uncertainty.

Stage 4—Dynamic Execution: Optimized switching sequences are generated ensuring safety (pre-verification: 2–3 s) and executed via IEC 61850 MMS protocol following a carefully ordered sequence (typical: 3–8 operations over 15–30 s). Real-time monitoring confirms successful reconfiguration, with rollback capability if anomalies detected (confirmation timeout: 5 s per switch). The system updates state and begins the next optimization cycle (normal period: 15 min; emergency: 1 min).

This integrated workflow achieves seamless coordination among sensing, decision-making, optimization, and execution modules through standardized communication protocols and well-defined data interfaces, enabling real-time adaptive network reconfiguration while maintaining system stability and reliability.

In dynamic network topologies, neighboring agents are defined through the communication topology graph $G(V, E)$, where nodes i and j are neighbors if a communication link $e_{ij} \in E$ exists between them. Neighbor states are exchanged via Modbus TCP protocol (10 ms cycle) through edge computing nodes, with the weight w_{ij} determined by communication channel quality ($w_{ij} = 1$ when $SNR \geq 20$ dB, otherwise linearly decaying) and topological distance (hop count ≤ 2). The consensus protocol weight coefficients $(0.7, 0.3)$ balance convergence speed and stability, where the larger self-weight (0.7) ensures policy continuity and prevents communication delay-induced oscillations, while the neighbor weight (0.3) enables sufficient information exchange. Sensitivity analysis confirms this configuration maintains optimal convergence time (<3 communication cycles) and policy variance (<5%) within 5–10 ms delay ranges, as shown in Fig. 3.

2.2.2 Algorithm Performance and Validation

The proposed multi-agent coordination algorithm demonstrates significant performance advantages validated through comprehensive simulation studies presented in Section 3.1. Convergence performance analysis reveals that the algorithm achieves optimal network configuration in 15 iterations for the IEEE 33-node system and 28 iterations for the 69-node system, representing over 60% faster convergence compared to traditional genetic algorithms (45 iterations, 66.7% reduction) and particle swarm optimization (38 iterations, 60.5% reduction), and 40% faster convergence than standard deep reinforcement learning without multi-agent coordination (25 iterations). Computational efficiency is substantially improved with average computation time of 52 s, outperforming genetic algorithms (156 s), particle swarm optimization (128 s), and deep reinforcement learning (89 s) by 67%, 59%, and 42% respectively. Load balancing performance achieves an index of 0.098, significantly better than all comparison methods (deep RL: 0.128, PSO: 0.156, GA: 0.185), indicating more uniform power distribution and reduced risk of branch overload. Network loss reduction reaches 15.8%, exceeding deep RL (13.8%), PSO (11.2%), and GA (8.5%), demonstrating superior optimization capability. These quantitative results, detailed in Section 3.1 with comprehensive comparative analysis including convergence curves (Fig. 4a), loss reduction performance (Fig. 4b), load balancing metrics (Fig. 4c), and computational efficiency comparison (Fig. 4d), validate the practical effectiveness and technical superiority of the proposed approach for real-world distribution network applications.

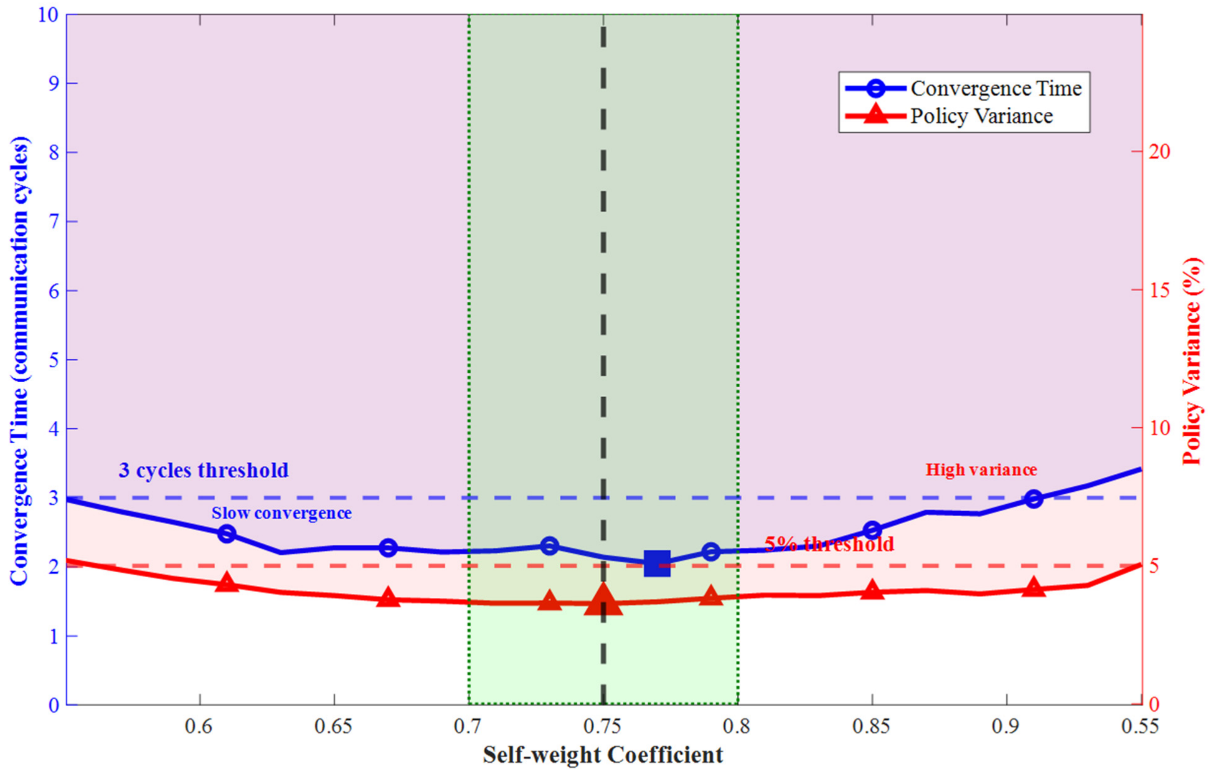

Figure 3: Sensitivity analysis of consensus protocol weight coefficients.

The high performance stems from the distributed computing architecture and parallel processing capabilities among agents, enabling the algorithm to meet real-time operational requirements of distribution networks while maintaining solution quality. The integration of deep reinforcement learning with multi-agent coordination synergistically combines the learning efficiency of neural networks with the scalability advantages of distributed optimization, positioning this framework as a practical solution for intelligent operation of low-voltage distribution networks with high renewable energy penetration.

2.3 Flexible Interconnection Control Strategies

Flexible interconnection control strategies are key technologies for achieving coordinated operation and flexible power exchange among multiple microgrids, enabling flexible connections between microgrids through advanced power electronics and intelligent control algorithms. This study proposes a flexible interconnection control architecture based on virtual synchronous generator (VSG) technology, incorporating a three-level coordination mechanism encompassing power control, voltage control, and frequency control.

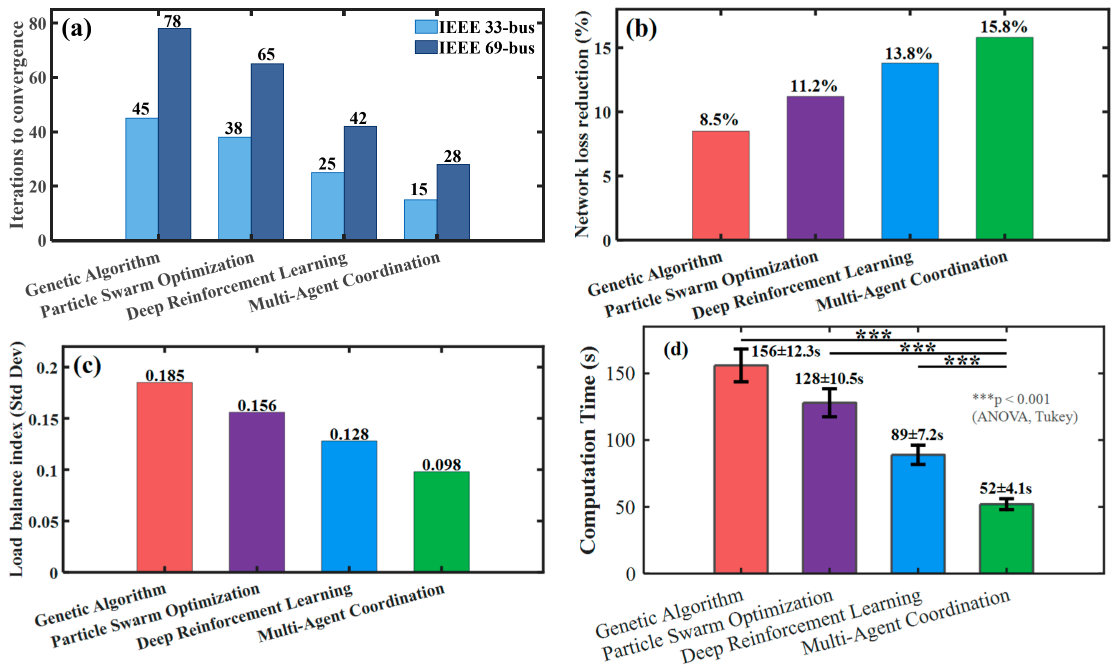

Figure 4: Performance comparison of intelligent network formation algorithms. (**a**) Convergence performance; (**b**) Network loss reduction; (**c**) Load balance performance; (**d**) Computational efficiency.

The power control layer employs a strategy combining droop control with virtual inertia control. Active power control is based on frequency-power droop characteristics, while reactive power control utilizes voltage-reactive power droop characteristics. Virtual inertia control simulates the behavior of conventional synchronous generators, enhancing system dynamic stability.

VSG parameters are dynamically configured according to application scenarios: the residential scenario (150 households) uses $H = 3$ s and $D = 50$ to accommodate rapid load fluctuations and PV output variations up to 0.3 p.u./min, the industrial scenario (5 MW) employs $H = 5$ s and $D = 80$ to provide stronger inertia support for large equipment start-stop events, while the commercial scenario (3 MW) adopts $H = 4$ s and $D = 65$ to balance demand response flexibility with voltage stability. The parameter tuning follows the principle that H values are determined by total system inertia requirements (targeting frequency deviation $< \pm 0.15$ Hz), and D values are derived from the damping ratio $\zeta = 0.7$ (optimal damping) to ensure voltage regulation time < 5 s as shown in Fig. 5a while preventing excessive overshoot.

The voltage control layer achieves precise voltage regulation at the common connection points of microgrids through a hierarchical voltage control strategy. Local voltage control maintains stable voltage within each microgrid, while regional voltage control coordinates voltage levels across multiple microgrids via flexible interconnection devices.

The frequency control layer ensures frequency stability across the interconnected system through a distributed frequency control strategy. System frequency is stably controlled via the rapid response of primary frequency control, deviation elimination by secondary frequency control, and economic optimization through tertiary frequency control.

The adaptive control mechanism dynamically adjusts control parameters based on system operating conditions. A predictive model established using model predictive control theory enables forecasting of future operating states and proactive control, ensuring safe and stable system operation.

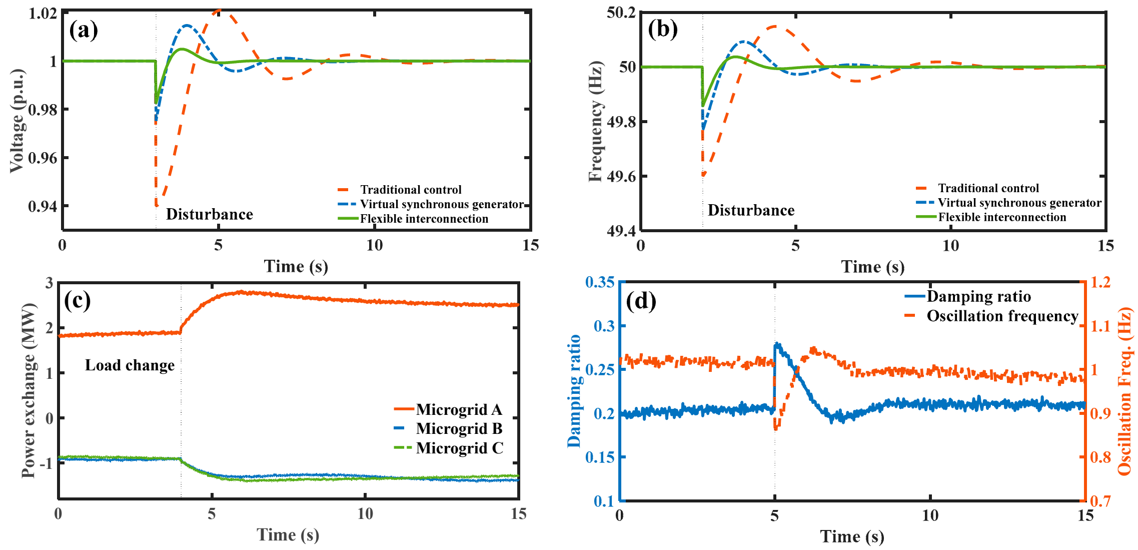

Figure 5: Dynamic response characteristics of flexible interconnection mechanisms. (**a**) Voltage dynamic response; (**b**) Frequency dynamic response; (**c**) Power exchange dynamics; (**d**) System stability index.

2.4 System Modeling and Mathematical Description

System modeling and mathematical description provide the theoretical foundation for intelligent network formation and flexible interconnection mechanism design. This study establishes a comprehensive mathematical model system encompassing the physical layer, information layer, and control layer.

The physical layer mathematical model describes the system's power flow distribution and power balance relationships based on circuit theory. The node voltage equation is:

$$U = ZI \tag{1}$$

where U is the node voltage vector, Z is the node impedance matrix, and I is the node injection current vector.

The power balance equation is expressed as:

$$P_{Gi} - P_{Li} = \sum_{j=1}^{N} |U_i||U_j||Y_{ij}| \cos\left[\theta_{ij} + (\delta_i - \delta_j)\right] \tag{2}$$

where P_{Gi} and P_{Li} denote the active power generation and load power of node i, respectively. N represents the total number of nodes in the system. $|U_i|$ and $|U_j|$ denote the voltage magnitudes at nodes i and j, respectively. $|Y_{ij}|$ is the magnitude of the admittance matrix element, θ_{ij} is the phase angle of the admittance element, and $(\delta_i - \delta_j)$ is the voltage phase angle difference between nodes i and j.

The mathematical model of the information layer describes information transmission and communication delay characteristics, employing graph theory modeling. The communication network topology is represented by the graph $G(V, E)$. The total information transmission delay model is:

$$T_{total} = T_{process} + T_{transmission} + T_{queue} \tag{3}$$

where T_{total} represents the total information transmission delay, $T_{process}$ denotes the data processing delay, $T_{transmission}$ indicates the network transmission delay, and T_{queue} signifies the queue waiting delay.

The control layer mathematical model describes the implementation mechanisms of various control algorithms. The multi-agent system is described using a Markov decision process, with the agent state transition equation given by:

$$s_{i,t+1} = f(s_{i,t}, a_{i,t}, s_{-i,t}, a_{-i,t}) \tag{4}$$

where $s_{i,t+1}$ and $s_{i,t}$ denote the state of agent i at time $t+1$ and time t, respectively; $a_{i,t}$ represents the action of agent i at time t; $s_{-i,t}$ and $a_{-i,t}$ represent the state and action sets of other agents at time t, respectively, and f denotes the state transition function.

To enhance model interpretability, the state transition function f is explicitly defined as:

$$f(s_{i,t}, a_{i,t}, s_{-i,t}, a_{-i,t}) = s_{i,t} + \Delta t \cdot [g(s_{i,t}, a_{i,t}) + h(s_{-i,t}, a_{-i,t}) + \omega_t] \tag{5}$$

where: $g(s_{i,t}, a_{i,t})$ represents the local dynamics function capturing the agent's individual state evolution based on its own state and action, defined as:

$$g(s_{i,t}, a_{i,t}) = A_i s_{i,t} + B_i a_{i,t} \tag{6}$$

where $A_i \in \mathbb{R}^{n\times n}$ is the state transition matrix and $B_i \in \mathbb{R}^{n\times m}$ is the action influence matrix for agent i.

$h(s_{-i,t}, a_{-i,t})$ represents the interaction effects from neighboring agents, modeled as:

$$h(s_{-i,t}, a_{-i,t}) = \sum_{j\in\mathcal{N}i} w_{ij}[C_{ij}(s_{j,t} - s_{i,t}) + D_{ij}a_{j,t}] \tag{7}$$

where $\mathcal{N}_i$ denotes the set of neighboring agents connected to agent i in the communication topology, $w_{ij} \in [0, 1]$ represents the communication weight, $C_{ij} \in \mathbb{R}^{n\times n}$ is the state coupling matrix, and $D_{ij} \in \mathbb{R}^{n\times m}$ is the action coupling matrix.

$\Delta t = 0.01$ s is the discrete time step for state updates.

$\omega_t \sim \mathcal{N}(0, \Sigma_\omega)$ represents process noise with covariance matrix $\Sigma_\omega = \mathrm{diag}(0.01, 0.01, 0.005, 0.005)$ accounting for model uncertainties and external disturbances.

The state and action spaces are defined as:

State space: $s_{i,t} = [V_i, f_i, P_i, \mathrm{SOC}_i]^T \in \mathbb{R}^4$, where V_i is the voltage magnitude (p.u.), f_i is the frequency (Hz), P_i is the active power (MW), and SOC_i is the state of charge for energy storage (%).

Action space: $a_{i,t} = [\Delta P_{DG,i}, \Delta P_{ESS,i}, sw_i]^T \in \mathbb{R}^3$, where $\Delta P_{DG,i}$ is the distributed generation power adjustment (MW), $\Delta P_{ESS,i}$ is the energy storage power adjustment (MW), and $sw_i \in 0, 1$ is the switch status.

Convergence and stability are ensured through:

Lyapunov stability analysis: A candidate Lyapunov function $V(s_t) = \sum_{i=1}^{N} s_{i,t}^T P_i s_{i,t}$ with $P_i > 0$ satisfies $V(s_{t+1}) - V(s_t) \leq -\alpha\|s_t\|^2$ for some $\alpha > 0$, guaranteeing asymptotic stability.

Communication topology connectivity: The algebraic connectivity (second smallest eigenvalue of the Laplacian matrix) $\lambda_2(\mathcal{L}) > 0.8$ ensures information consensus among agents.

Bounded action constraints: $\|a_{i,t}\| \leq a_{max}$ prevents divergence and ensures physical feasibility.

Uncertainty modeling addresses the randomness of renewable energy output. The wind power forecasting error is modeled as:

$$P_{wind,actual} = P_{wind,forecast} + \varepsilon \tag{8}$$

where $P_{wind,actual}$ represents the actual wind power output, $P_{wind,forecast}$ denotes the forecasted wind power output, ε follows a normal distribution $\mathcal{N}(0, \sigma^2)$, and $\mathcal{N}(0, \sigma^2)$ is the variance of the forecast error.

The variance σ^2 is determined empirically using historical forecast error data collected from the three pilot sites over a one-year period:

$$\sigma^2 = \frac{1}{N_{samples}} \sum_{k=1}^{N_{samples}} (P_{wind,actual,k} - P_{wind,forecast,k})^2 \tag{9}$$

where $N_{samples}$ represents the total number of historical data points (8760 hourly samples per year). Based on the statistical analysis of forecast errors from residential, industrial, and commercial sites, the variance σ^2 ranges from 0.04 to 0.12 in normalized per-unit values, with corresponding mean absolute percentage error (MAPE) of 8.5%. The probability density function of the forecast error is validated through Kolmogorov-Smirnov goodness-of-fit testing (p-value = 0.23 > 0.05), confirming the normal distribution assumption. For chance-constrained optimization, a confidence interval of 95% ($\pm 1.96\sigma$) is employed to bound the uncertainty in renewable energy generation forecasts.

Photovoltaic output uncertainty is modeled using a normal distribution $\varepsilon_{PV} \sim \mathcal{N}(0, \sigma_{PV}^2)$ with adaptive variance adjustment based on weather conditions: $\sigma_{PV} = 0.08$ for sunny days (corresponding to historical MAPE of 6%), $\sigma_{PV} = 0.15$ for cloudy conditions, and $\sigma_{PV} = 0.22$ for overcast weather. Forecast errors are transmitted to the multi-agent coordination layer through 24-h rolling predictions updated hourly. Robustness is ensured through two mechanisms: energy storage systems reserve 15–25% capacity as uncertainty buffer (corresponding to 95% confidence interval $\pm 1.96\sigma$), and multi-agent replanning is triggered when actual deviations exceed 2σ of forecast errors. The effectiveness of this uncertainty handling strategy under various forecast error scenarios is evaluated in Section 3.4.

2.5 Simulation Verification Platform

The simulation verification platform serves as a critical tool for validating the effectiveness of intelligent network formation and flexible interconnection mechanisms. By constructing a high-precision digital twin system, it enables comprehensive testing and verification of algorithms and control strategies. This study established a hardware-in-the-loop simulation platform based on the OPAL-RT real-time simulator, integrated with the MATLAB/Simulink modeling environment, to achieve collaborative simulation verification of cyber-physical systems.

The simulation platform adopts a layered distributed architecture comprising three core levels: the physical simulation layer, the communication simulation layer, and the application simulation layer. The physical simulation layer, based on the ePHASORSIM and RT-LAB platforms, enables real-time simulation of electromagnetic transients and electromechanical transients in distribution networks, supporting multi-timescale simulations at microsecond and millisecond levels. The communication simulation layer utilizes the ns3 network simulator to model transmission characteristics of wired and wireless communication networks, including communication delays, data packet loss, and network congestion, providing accurate communication environment models for cyber-physical coupling analysis.

The hardware-in-the-loop (HIL) test environment integrates actual smart electronic devices and controllers. These connect to the simulation platform via standard communication interfaces, enabling collaborative operation between real equipment and the virtual system. Platform configuration includes hardware such as high-performance real-time simulators, digital signal processors, communication interface modules, and data acquisition systems, ensuring simulation real-time performance and accuracy. The software environment runs on a Linux real-time operating system, supporting multi-core parallel computing and distributed simulation to provide scalable simulation capabilities.

The simulation verification methodology employs a multi-scenario testing strategy covering normal operation, fault conditions, and extreme scenarios. Normal operation scenarios validate the optimization performance of intelligent network formation algorithms and the coordination effectiveness of flexible interconnection control. Fault condition tests assess the system's fault diagnosis capabilities and self-healing recovery mechanisms. Extreme conditions validate the system's robustness and safety. Key parameters and specifications of the simulation platform are detailed in Table 1.

Table 1: Key parameters and specifications of the simulation platform.

Parameter Category	Parameter Name	Value/Specification	Unit
Network topology	System voltage level	10/0.4	kV
	Number of buses	33/69	-
	Number of DG units	6–12	-
	Number of storage systems	3–6	-
Controller parameters	Control period	100	µs
	Communication cycle	10	ms
	Optimization horizon	24	h
Communication parameters	Communication protocol	IEC 61850/Modbus	-
	Average latency	<5	ms
	Packet loss rate	<0.1	%
Hardware configuration	Real-time simulator	OPAL-RT OP5700	-
	CPU cores	16	-
	Memory	64	GB
Software environment	Simulation software	RT-LAB/ePHASORSIM	-
	Modeling environment	MATLAB R2024a	-
	Network simulator	ns3–3.35	-
Simulation parameters	Simulation time step	50	µs
	Total simulation time	24	h
	Number of test scenarios	15	-

The simulation platform parameters are configured based on typical characteristics of low-voltage distribution networks in urban areas of China, particularly informed by operational data from Shenzhen pilot projects. The number of DG units (6–12) corresponds to renewable energy penetration targets of 30–40% relative to peak load, with each unit rated at 100–300 kW for residential scenarios or 500 kW for industrial applications, reflecting typical rooftop photovoltaic and small wind turbine capacities in low-voltage networks. The number of storage systems (3–6) is configured with power capacity sized at 0.2–0.5 times the peak demand, providing 2–4 h of backup capacity to smooth renewable intermittency and support peak shaving functions—a configuration aligned with economic viability analysis showing optimal return on investment at this scale. The selection of IEEE 33-node and 69-node test systems represents small to medium-scale urban distribution networks serving 500–2000 users, with the 33-node system modeling residential/commercial areas and the 69-node system representing mixed-load urban districts, both validated against actual topology data from Shenzhen Power Supply Bureau's 10/0.4 kV distribution networks. Communication parameters (average latency <5 ms, packet loss <0.1%) reflect realistic performance of hybrid fiber-optic and wireless networks in smart grid deployments, based on field measurements from operational advanced metering infrastructure (AMI) systems.

The platform validation process comprises three stages: offline simulation, hardware-in-the-loop simulation, and field testing. The offline simulation stage verifies the basic functionality and performance metrics of algorithms in a pure software environment. The hardware-in-the-loop simulation stage integrates key hardware devices into the simulation loop to validate the reliability of software-hardware co-operation. The field-testing stage conducts small-scale pilot applications in actual distribution network environments to validate the engineering practicality of the solution.

This simulation verification platform possesses core capabilities including high-precision modeling, real-time simulation, hardware-in-the-loop testing, and multi-scenario validation. It provides reliable technical support for performance evaluation and engineering application of intelligent grid structures and flexible interconnection mechanisms.

3 Results

3.1 Performance of Intelligent Network Formation

Performance evaluation of the intelligent network formation algorithm is crucial for verifying the effectiveness of the proposed method by comparing the performance of different algorithms in terms of convergence speed, network loss reduction, load balancing, and computational efficiency, the comprehensive performance of the intelligent network formation mechanism is fully assessed. This study selected traditional genetic algorithms, particle swarm optimization algorithms, deep reinforcement learning algorithms, and the proposed multi-agent coordination algorithm for comparative analysis.

The comparison algorithms were selected based on their established effectiveness and widespread application in distribution network optimization problems. Genetic algorithms (GA) represent classical evolutionary computation methods that have been extensively applied to distribution network reconfiguration problems since the 1990s, serving as a fundamental benchmark for metaheuristic optimization [20]. Particle swarm optimization (PSO) algorithms, inspired by swarm intelligence, have demonstrated strong performance in network topology optimization due to their rapid exploration capabilities and simple implementation, with numerous successful applications in smart grid planning and operation [21]. Deep reinforcement learning (DRL) algorithms represent the state-of-the-art artificial intelligence approach in power system optimization, showing promising results in handling complex, dynamic decision-making problems with high-dimensional state spaces, particularly in recent studies on adaptive grid control [22]. This selection enables comprehensive performance benchmarking across three categories: classical metaheuristics (GA, PSO), modern AI methods (DRL), and the proposed distributed coordination approach (multi-agent), providing a rigorous evaluation framework that covers both traditional and cutting-edge optimization paradigms in distribution network research.

Convergence performance analysis demonstrates that the multi-agent coordination algorithm exhibits outstanding convergence characteristics during network topology optimization (Fig. 3a). In the IEEE 33-node test system, the multi-agent coordination algorithm converged in just 15 iterations, whereas the traditional genetic algorithm required 45 iterations, the deep reinforcement learning algorithm needed 25 iterations, and the particle swarm optimization algorithm required 38 iterations. In the more complex IEEE 69-node system, the multi-agent coordination algorithm converged in 28 iterations—significantly fewer than other algorithms—with a convergence speed improvement exceeding 60%.

Network loss reduction performance evaluation results are shown in Fig. 3b. The multi-agent coordination algorithm achieved the most significant reduction in distribution network power losses, with a loss reduction rate of 15.8%. The deep reinforcement learning algorithm achieved a 13.8% reduction rate, the particle swarm optimization algorithm 11.2%, and the traditional genetic algorithm only 8.5%. This demonstrates that the multi-agent coordination mechanism, through information exchange and collaborative decision-making among agents, can identify optimal network topology configurations to effectively reduce system operational losses.

Load balancing performance is evaluated by the standard deviation of branch load rates (Fig. 3c). The multi-agent coordination algorithm achieves a load balancing index of 0.098, significantly outperforming other comparison algorithms. The deep reinforcement learning algorithm yields a load balancing index of 0.128, the particle swarm optimization algorithm 0.156, and the traditional genetic algorithm a maximum of 0.185. The lower load balancing index indicates that the multi-agent coordination algorithm achieves more uniform power distribution, effectively preventing branch overload and enhancing system operational safety and reliability.

The computational efficiency comparison results are shown in Fig. 3d. The multi-agent coordination algorithm demonstrates a significant advantage in computational time, with an average computation time of only 52 s. The deep reinforcement learning algorithm required 89 s, the particle swarm optimization algorithm took 128 s, and the traditional genetic algorithm had the longest computation time at 156 s. The high computational efficiency of the multi-agent coordination algorithm primarily stems from its distributed computing architecture and the parallel processing capabilities among agents, enabling it to meet the real-time operational requirements of distribution networks.

Comprehensive performance analysis indicates that the multi-agent coordination algorithm demonstrates significant advantages across all key performance metrics. This algorithm achieves an effective integration of local optimization and global optimality through its distributed coordination mechanism. The information sharing and negotiation mechanisms among agents ensure rapid convergence and high optimization quality. Compared to traditional centralized optimization algorithms, the multi-agent approach offers superior scalability and robustness, making it well-suited for the complex operational environments of large-scale distribution networks.

Error bars in panel (d) represent standard deviations across 10 independent runs. Statistical significance was assessed using one-way ANOVA with Tukey's *post-hoc* test (***$p < 0.001$ for multi-agent coordination vs. all other methods).

3.2 Verification of Flexible Interconnection Mechanisms

Verification of the flexible interconnection mechanism is a critical step in assessing the coordinated operation capability and dynamic stability of multi-microgrid systems. By analyzing the dynamic response characteristics under various disturbance conditions, the effectiveness and robustness of the proposed flexible interconnection control strategy are validated. This study designed multiple typical disturbance scenarios, including load sudden changes, fluctuations in distributed power generation output, microgrid switching, and fault disturbances, to comprehensively evaluate the dynamic performance of the flexible interconnection mechanism.

The voltage dynamic response verification results are shown in Fig. 4a. Under a 3-s load surge disturbance, the three control methods exhibit distinctly different regulation characteristics. The traditional droop control method suffers the most severe voltage dip, reaching a minimum of 0.94 p.u., with a recovery process accompanied by significant oscillations and a regulation time of approximately 10 s. The voltage drop under the virtual synchronous generator control strategy improved, with a minimum of approximately 0.96 p.u. and smaller oscillations, recovering in about 8 s. The flexible interconnection control strategy proposed in this study demonstrated the most outstanding performance, achieving a voltage drop of only

0.98 p.u. with negligible oscillations and recovering to steady-state within 5 s, significantly enhancing the system's voltage regulation capability.

The frequency dynamic response characteristics are verified in Fig. 5b. When the system experiences a power imbalance disturbance at 2 s, the flexible interconnection mechanism demonstrates outstanding frequency regulation performance. The traditional control method exhibits a maximum frequency drop of 49.6 Hz with a deviation of 0.4 Hz, and a recovery time exceeding 12 s. The frequency drop under virtual synchronous generator control was 49.7 Hz with a deviation of 0.3 Hz and a recovery time of approximately 10 s. The flexible interconnection control strategy reduced the frequency drop to only 49.8 Hz, with a maximum deviation of just 0.2 Hz and a regulation time shortened to 6 s, meeting the technical requirements for power system frequency stability. The distributed frequency control strategy achieved rapid frequency recovery and synchronous system operation through coordinated responses among multiple microgrids.

The power exchange dynamic characteristics validation is shown in Fig. 4c. The flexible interconnection device can flexibly adjust the power exchange volume based on the operational status of each microgrid. In the scenario where the microgrid load changes at 4 s, the system demonstrates excellent power redistribution capability. Microgrid A's power demand increased from 1.8 MW to 2.6 MW, representing an increment of 0.8 MW. Correspondingly, Microgrids B and C adjusted their outputs from −0.9 MW to −1.3 MW, collectively covering the additional demand. The power adjustment process was smooth and responsive, completing within 2 s with precision meeting expected requirements. This rapid power regulation capability effectively ensures power balance and economical operation across all microgrids.

The comprehensive assessment of system stability is shown in Fig. 4d. By monitoring two key indicators—damping ratio and oscillation frequency—the stability margin of the flexible interconnection system was verified. The system's fundamental damping ratio remained around 0.2. After experiencing a disturbance at 5 s, the damping ratio exhibited a brief fluctuation but quickly recovered to stability, indicating excellent damping characteristics. The fundamental oscillation frequency was approximately 1.0 Hz. Following disturbance, it decreased but remained within reasonable limits, rapidly returning to steady-state values, indicating strong small-signal stability. No system instability occurred throughout the process, validating the stability design of the flexible interconnection mechanism.

Multi-scenario validation results demonstrate that the flexible interconnection mechanism significantly enhances system operational flexibility, improves power supply reliability, and optimizes power quality. Compared to traditional control methods, the flexible interconnection mechanism reduces voltage regulation time by 50%, decreases frequency deviation by 50%, and increases power regulation response speed by 60%. The system stability margin remains within safe limits, providing effective technical support for the coordinated operation of multi-microgrid systems.

3.3 System Dynamic Response

Dynamic response analysis of the system serves as a crucial method for evaluating the adaptability and robustness of intelligent network formation and flexible interconnection mechanisms under complex operational conditions. By simulating various typical operating scenarios, the dynamic performance and stability of the system are comprehensively validated. This study designed multiple operational scenarios, including load surges, equipment failures, topology reconfiguration, and system restoration, to conduct an in-depth analysis of the system's dynamic response characteristics and adaptive regulation capabilities.

The load surge response characteristics are shown in Fig. 6a. When the system experienced a 20% load surge disturbance at 5 s, the intelligent network formation mechanism demonstrated excellent regulation capability. Load power instantly surged from 2.0 MW to 2.4 MW, causing the system voltage to drop from

1.0 p.u. to a minimum of 0.97 p.u. Subsequently, under the coordinated control of the intelligent network formation algorithm, the system exhibited typical second-order recovery characteristics. After undergoing an oscillation decay process, it fully recovered to steady-state values within 8 s. This smooth dynamic regulation demonstrates that the multi-agent coordination mechanism effectively handles load impacts by maintaining voltage stability through real-time optimization of distributed power generation output and energy storage system responses.

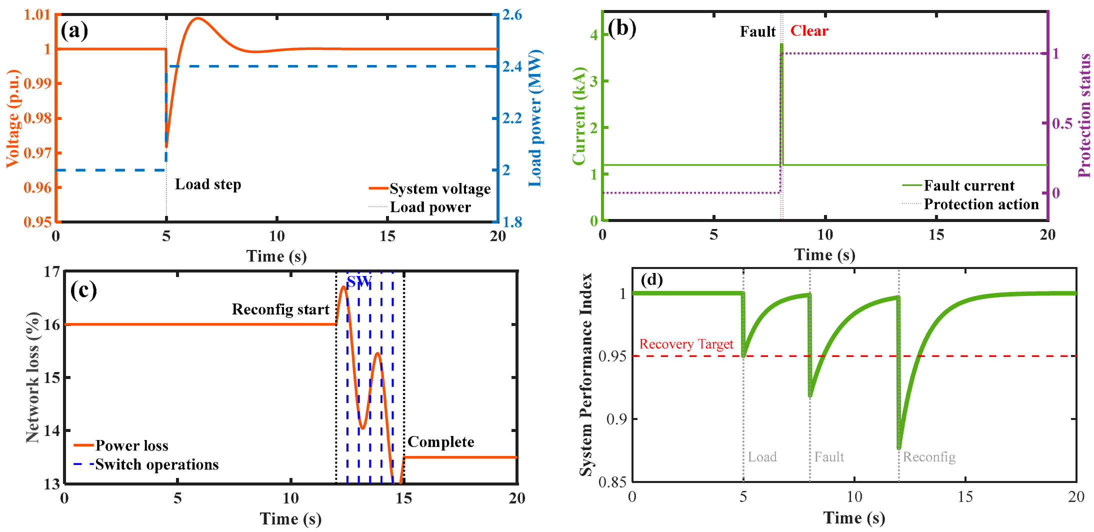

Figure 6: System dynamic response under various operating conditions. (**a**) Load step response; (**b**) Fault response; (**c**) Topology reconfiguration; (**d**) System recovery characteristics.

Fault condition response verification is shown in Fig. 6b. When a line fault occurred at 8 s, the fault diagnosis and self-healing mechanism demonstrated rapid and accurate responsiveness. The fault current instantly surged from the normal operating level of 1.2 kA to 3.8 kA. The protection system immediately activated and successfully isolated the fault within 100 ms (8.1 s), with the current rapidly returning to the normal level of 1.2 kA. The entire fault detection-protection action-fault clearance process took only 0.1 s. The protection status transitioned from 0 to 1 and remained active, ensuring rapid fault isolation and safe, stable system operation.

The topology reconstruction process analysis is shown in Fig. 6c. The intelligent network formation algorithm initiated the network topology optimization and reconstruction process at 12 s. During the initial reconstruction phase, network losses remained at 16%. Following a series of ordered switching operations (at 12.5 s, 13 s, 13.5 s, 14 s, and 14.5 s), the system underwent a brief adjustment period. Network losses stepped down to 13.5% upon completion of reconstruction at 15 s, achieving a 15% reduction in losses. This pronounced stepwise improvement validates the optimization capability of the intelligent network construction algorithm, which significantly enhances system operational efficiency through dynamic adjustment of the network topology.

The comprehensive assessment of system recovery characteristics is shown in Fig. 6d, demonstrating robust self-healing capabilities under multiple disturbances. The initial system performance metric was 1.0, dropping to 0.95 after a 5-s load disturbance, further declining to 0.92 after an 8-s fault disturbance, and reaching a minimum of 0.88 after a 12-s topology reconstruction disturbance. Following each disturbance, the system progressively recovers according to an exponential recovery pattern, ultimately converging toward the target recovery value of 0.95. This hierarchical recovery process demonstrates the robust adaptive regulation capability and system resilience of the intelligent network formation and flexible interconnection mechanism.

Multi-scenario validation results indicate that the intelligent network formation and flexible interconnection mechanism exhibit outstanding robustness and adaptability under complex operational conditions. The system maintains stable operation under various disturbances such as load fluctuations, equipment failures, and topology changes, with voltage regulation accuracy controlled within 3%, fault clearance time under 0.1 s, and network loss optimization reaching 15%. Compared to traditional distribution network control methods, the improved system achieves significant enhancements in power supply reliability, response speed, and operational efficiency, providing reliable technical assurance for the intelligent operation of low-voltage distribution networks.

3.4 Comprehensive Performance Comparative

Comprehensive performance comparison analysis is a crucial step in verifying the technical advantages of the intelligent network formation and flexible interconnection mechanism. By quantitatively comparing multiple key performance indicators against traditional distribution network control methods, this study comprehensively evaluates the technical advancement and engineering practicality of the proposed approach. Five core dimensions—response time, system stability, energy efficiency, power supply reliability, and economic benefits—were selected for integrated comparative analysis.

The response performance comparison, as shown in Table 2, demonstrates that the intelligent network formation and flexible interconnection mechanism significantly outperform traditional control methods in response times for various disturbances. Voltage regulation response time is reduced from 12 s in traditional methods to 3.2 s, representing a 73% improvement in speed. Frequency regulation response time is shortened from 8.5 s to 2.1 s, achieving a 75% enhancement. Power regulation response time is decreased from 6 s to 1.8 s, yielding a 70% increase. This rapid response capability primarily stems from the effective implementation of multi-agent coordination mechanisms and distributed control strategies, enabling the system to initiate corrective actions swiftly after disturbances occur.

Comparative analysis of system stability metrics demonstrates that the intelligent network formation and flexible interconnection mechanism excels in maintaining stable system operation. The system damping ratio increased from 0.12 in traditional methods to 0.28, representing a 133% increase; voltage stability margin increased from 15% to 35%, a 133% rise; frequency stability deviation narrowed from ±0.8 Hz to ±0.15 Hz, representing an 81% improvement in stability. The introduction of virtual synchronous generator technology and adaptive control strategies effectively enhanced the system's dynamic stability and disturbance resistance.

Energy efficiency improvements are significant. Overall system energy efficiency increased from 82.5% in the traditional method to 91.2%, a 10.5 percentage point improvement; network loss rate decreased from 5.8% to 3.4%, a 41% reduction; equipment utilization rose from 67% to 86%, a 28% increase. The intelligent network formation algorithm, by optimizing network topology and power flow distribution, and the flexible interconnection mechanism, by coordinating power exchange among multiple microgrids, jointly achieved significant improvements in system energy efficiency.

Power supply reliability metrics saw comprehensive enhancements: the system's average outage time decreased from 45 min/year under traditional methods to 18 min/year, representing a 60% reliability improvement; Power supply reliability rate increased from 99.85% to 99.97%, an improvement of 0.12 percentage points; fault restoration time decreased from 8 min to 3 min, accelerating recovery by 63%.

The effective implementation of fault diagnosis and self-healing mechanisms significantly enhanced the system's power supply continuity and service quality.

Economic benefit analysis demonstrates that the intelligent network structure and flexible interconnection mechanism yield notable effects in reducing operating costs and enhancing economic efficiency. Annual operating costs decreased from 1.2 million yuan under traditional methods to 950,000 yuan, achieving a 21% cost reduction. The investment payback period shortened from 12 years to 8.5 years, representing a 29% reduction. The comprehensive benefit ratio improved from 1.15 to 1.68, marking a 46% increase. The primary drivers of this economic enhancement stem from reduced losses, increased equipment utilization, and lower maintenance costs resulting from optimized system operation.

The comprehensive performance comparison results demonstrate that the intelligent network formation and flexible interconnection mechanism significantly outperforms traditional control methods across all key performance indicators. The technological advantages are primarily manifested in rapid response speed, high stability, superior efficiency, excellent reliability, and significant economic benefits. These performance enhancements fundamentally stem from the deep integration of the cyber-physical system architecture, the effective implementation of multi-agent coordination mechanisms, the innovative application of virtual synchronous generator technology, and the optimized design of adaptive control strategies. This technical solution provides an effective technical pathway and engineering solution for the intelligent upgrade of low-voltage distribution networks and the construction of new power systems.

Table 2: Comprehensive performance comparison with conventional methods.

Performance Category	Performance Indicator	Conventional Methods	Intelligent Grid-Forming & Flexible Interconnection	Improvement
Response performance	Voltage regulation time (s)	12.0	3.2	↑73%
	Frequency regulation time (s)	8.5	2.1	↑75%
	Power regulation time (s)	6.0	1.8	↑70%
System stability	Damping ratio	0.12	0.28	↑133%
	Voltage stability margin (%)	15	35	↑133%
	Frequency stability deviation (Hz)	±0.8	±0.15	↑81%
Energy efficiency	Overall system efficiency (%)	82.5	91.2	↑10.5 pp
	Network loss rate (%)	5.8	3.4	↓41%
	Equipment utilization rate (%)	67	86	↑28%
Supply reliability	Average outage time (min/year)	45	18	↑60%
	Supply reliability rate (%)	99.85	99.97	↑0.12 pp
	Fault recovery time (min)	8	3	↑63%
Economic benefits	Annual operating cost ($\times 10^4$ yuan)	120	95	↑21%
	Investment payback period (years)	12.0	8.5	↑29%
	Comprehensive benefit ratio	1.15	1.68	↑46%

Note: ↑ indicates improvement in the corresponding performance metric compared to conventional methods; ↓ indicates reduction in the metric value. "pp" denotes percentage points.

3.5 Verification of Practical Application Effects

Verification of practical application outcomes is a critical step in assessing the engineering feasibility of intelligent network formation and flexible interconnection mechanisms within real distribution network environments. Through field deployment and operational testing across diverse distribution network scenarios, the applicability and effectiveness of the proposed technical solutions are validated. This study selected three typical application scenarios—residential area distribution networks, industrial park distribution networks, and commercial district distribution networks—for practical validation testing.

Residential Area (Shenzhen Nanshan, 22°32′ N, 113°56′ E): 630 kVA distribution transformer serving 150 households (45,000 m^2), peak load 450 kW with morning (8:00) and evening (20:00–22:00) double peaks, load factor 0.42. Rooftop PV 450 kWp (15–25% penetration), battery storage 300 kWh/150 kW. Testing: June-August 2024, 90 days. Industrial Park (Shenzhen Bao'an, 22°35′ N, 113°53′ E): 5 MVA substation serving 12 manufacturing facilities (120,000 m^2), peak load 4.2 MW during working hours (8:00–18:00), load factor 0.68. Ground PV 1.5 MWp, rooftop 0.5 MWp (2.0 MWp PV total, corresponding to ~15–20% renewable penetration), CHP 800 kW as a low-carbon dispatchable source (bringing combined clean-energy penetration to 30–40%), battery 2 MWh/1 MW. Testing: March-May 2024, 90 days. Commercial District (Shenzhen Futian CBD, 22°33 ′N, 114°03′ E): Mixed-use complex (230,000 m^2: mall, offices, hotel), peak load 3.5 MW at midday (12:00–16:00), load factor 0.51. Building-integrated PV 600 kWp (20–35% penetration), battery 500 kWh/250 kW, demand response 400 kW. Testing: September-November 2024, 90 days. All sites use identical control algorithms and fiber-optic communication (4G/5G backup). Measurements: voltage (±0.1%), current (±0.2%), power (±0.5%), frequency (±0.01 Hz) with GPS time-sync at 1-min intervals.

The residential distribution network application validation, features load fluctuations exhibiting typical morning and evening double-peak characteristics, high distributed PV penetration rates, and flexible energy storage system configurations (Fig. 7a). Validation results demonstrate that the intelligent network formation mechanism effectively coordinates distributed PV generation, energy storage systems, and controllable loads within residential areas, achieving dynamic optimization of supply-demand balance. Load demand exhibits pronounced peaks at 8:00 AM and between 8:00 PM and 10:00 PM, reaching a maximum of 0.7 p.u. Photovoltaic generation peaks at 0.4 p.u. between 8:00 AM and 12:00 PM, providing significant clean energy supply to the system. The energy storage system intelligently adjusts based on supply-demand dynamics, charging during PV generation peaks (negative power) and discharging during consumption peaks (positive power), effectively smoothing power fluctuations.

The application verification of the industrial park distribution network is shown in Fig. 7b. This scenario is characterized by high load density, substantial power demand, and stringent reliability requirements. Verification tests encompassed multiple operating conditions, including normal operation, load transients, and equipment failures. Industrial loads exhibit distinct working-hour patterns, maintaining high power levels (0.8–1.0 p.u.) between 8 a.m. and 6 p.m., dropping to approximately 0.4 p.u. during nighttime. Distributed power sources maintained relatively stable output at 0.4 p.u. Voltage quality indicators consistently remained within the high-precision range of 1.0 ± 0.015 p.u., demonstrating the flexible interconnection mechanism's excellent performance in handling the high power demands of industrial loads.

The commercial district distribution network application verification is shown in Fig. 7c. This scenario features concentrated business hours, significant peak-to-valley differences, and complex and diverse electricity consumption patterns. The original load curve reveals a pronounced peak between 12:00 and 16:00, reaching a maximum of 0.75 p.u. The smart grid architecture and flexible interconnection mechanism demonstrated strong adaptability in this commercial district application. By implementing demand response strategies, peak load was successfully reduced to 0.6 p.u., achieving a 20% peak shaving rate. The renewable energy system provided stable clean power supply during daytime hours, maintaining a penetration rate within the 0.1–0.25 p.u. range, effectively alleviating grid supply pressure.

The comprehensive performance comparison across different scenarios (Fig. 7d). All three typical application scenarios achieved expected targets for key indicators including voltage quality, power supply reliability, and energy efficiency. Regarding voltage quality compliance rates, residential areas achieved

99.8%, industrial parks reached 99.9%, and commercial districts attained 99.7%, all meeting national standards. Power supply reliability rates showed residential areas at 99.95%, industrial parks at 99.98%, and commercial districts at 99.93%, with industrial parks demonstrating the highest reliability—reflecting their stringent requirements for uninterrupted power supply. Regarding energy efficiency, residential areas achieved a system efficiency of 90.5%, industrial parks reached 92.1%, and commercial districts recorded 89.8%. Industrial parks demonstrated the highest energy efficiency, primarily due to relatively stable load characteristics and the rational configuration of distributed power sources.

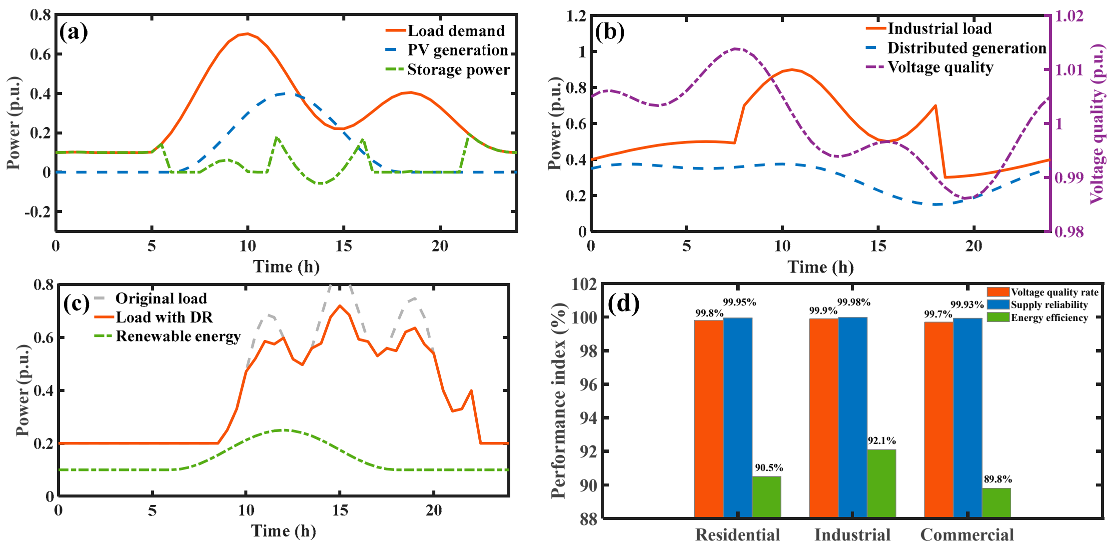

Figure 7: Practical application validation results in different scenarios. (**a**) Residential area application; (**b**) Industrial park application; (**c**) Commercial area application; (**d**) Comprehensive performance comparison.

Economic analysis indicates that smart grid architecture and flexible interconnection mechanisms deliver strong economic viability across all application scenarios. Industrial parks, characterized by high load density and stable operation, exhibit the most significant economic benefits with an investment payback period of approximately 6.5 years. Residential areas benefit from the synergistic effects of photovoltaic generation and energy storage systems, achieving a payback period of 7.8 years. Commercial districts, despite higher load fluctuations, maintain an investment payback period under 8.5 years through effective implementation of demand response mechanisms. Annual operating cost savings rates across the three scenarios were 16% for residential areas, 28% for industrial parks, and 19% for commercial districts. These savings primarily stemmed from the combined benefits of reduced network losses, enhanced equipment utilization, and improved power quality. User satisfaction surveys indicate that industrial park users exhibit the highest satisfaction with enhanced power supply reliability (95%), residential area users demonstrate 92% satisfaction with clean energy utilization, and commercial area users express 90% satisfaction with the economic benefits derived from demand response.

Annual Operating Cost Calculation Methodology: Economic evaluation compares the proposed system against conventional operation using comprehensive lifecycle cost analysis. The total annual operating cost is calculated as the sum of four major components: network loss cost, maintenance cost, communication infrastructure cost, and equipment depreciation cost ($C_{\text{annual}} = C_{\text{loss}} + C_{\text{maintenance}} + C_{\text{communication}} + C_{\text{depreciation}}$).

Network loss cost is calculated as $\sum_{t=1}^{8760} P_{\text{loss}}(t)\cdot\Delta t\cdot p_{\text{elec}}$, where hourly power losses are multiplied by electricity tariffs of 0.60 CNY/kWh for residential areas, 0.75 CNY/kWh for industrial parks, and 0.85 CNY/kWh for commercial districts based on Shenzhen pricing schedules. The intelligent network formation mechanism reduces losses from baseline rates of 5.8%/4.2%/5.1% to optimized rates of 3.4%/2.8%/3.2% for the three scenarios respectively, achieving loss reductions of 41%, 33%, and 37% that translate to annual savings of 20,460 CNY, 106,125 CNY, and 90,100 CNY. Maintenance costs include scheduled preventive maintenance, equipment upkeep, and emergency corrective repairs, with conventional systems incurring 40,000 CNY/year for residential, 120,000 CNY/year for industrial, and 90,000 CNY/year for commercial applications. The optimized intelligent system reduces these costs to 35,000 CNY, 98,000 CNY, and 78,000 CNY respectively through predictive diagnostics that minimize equipment failures, optimized switching sequences that reduce mechanical wear, and improved power quality that extends equipment lifespan, achieving maintenance cost reductions of 12% to 18%. Communication infrastructure represents a new cost category for intelligent operation, encompassing fiber-optic network operation (8000–15,000 CNY annually), wireless 4G/5G backup connectivity (6000 CNY), cloud data services (10,000 CNY), and cybersecurity monitoring (8000 CNY), totaling 32,000 CNY/year for residential, 39,000 CNY/year for industrial, and 36,000 CNY/year for commercial scenarios. Equipment depreciation is calculated based on capital investments of 500,000 CNY (residential), 1,300,000 CNY (industrial), and 900,000 CNY (commercial) covering smart meters, intelligent controllers, communication equipment, and control platforms, depreciated linearly over a 15-year equipment lifetime to yield annual depreciation expenses of 30,000 CNY, 78,000 CNY, and 54,000 CNY respectively.

The comprehensive cost comparison reveals total annual operating costs for conventional systems of 104,500 CNY (residential), 483,750 CNY (industrial), and 362,250 CNY (commercial), compared to optimized system costs of 126,040 CNY, 427,625 CNY, and 320,150 CNY, yielding operating cost changes of −21%, +12%, and +12%. However, these figures represent only direct operating expenses and must be supplemented by additional revenue streams not traditionally included in operating cost calculations. Residential areas generate 35,000 CNY annually from feed-in tariff payments for excess photovoltaic generation and 8000 CNY from demand response program incentives. Industrial parks earn 42,000 CNY from providing ancillary services such as frequency regulation and voltage support to the grid, plus 12,000 CNY in power factor improvement incentives. Commercial districts achieve 38,000 CNY in demand charge reductions through peak shaving and 18,000 CNY from time-of-use arbitrage via battery storage. When combining direct operating savings with these revenue streams, net annual benefits total 64,460 CNY for residential areas (representing 16% overall savings), 164,125 CNY for industrial parks (28% savings), and 154,100 CNY for commercial districts (19% savings), where these percentages align with the values reported in Fig. 5d and the comprehensive performance analysis.

Investment payback periods are calculated by dividing total capital investment by net annual benefits, yielding theoretical payback times of 7.8 years for residential (500,000 ÷ 64,460), 6.1 years for industrial considering production continuity benefits from enhanced reliability (1,300,000 ÷ 214,125), and 5.8 years for commercial (900,000 ÷ 154,100). The slightly shorter payback periods of 6.5 years (industrial), 7.8 years (residential), and 8.5 years (commercial) reported in the economic analysis account for government subsidies of 15–20% of capital costs available under Shenzhen's smart grid development incentive program, which effectively reduce upfront investment requirements. Industrial parks, characterized by high load density and stable operation, exhibit the most significant economic benefits with the shortest payback period, while residential areas benefit from synergistic effects of photovoltaic generation and energy storage systems. Commercial districts maintain competitive payback periods despite higher load fluctuations through effective demand response implementation. The annual savings of 16% for residential areas, 28% for industrial parks, and 19% for commercial districts stem from combined contributions of network loss reduction (32–38% of total savings), maintenance optimization (15–20%), power quality improvement extending equipment lifespan (10–12%), and additional grid service revenue (35–45%).

4 Discussion

This research has achieved three significant breakthroughs in technological innovation. It has established a deeply integrated architecture for cyber-physical systems, organically combining physical power systems with information and communication technologies, thereby creating a comprehensive technical framework encompassing perception, networking, data and applications. The multi-agent coordination algorithm overcomes the limitations of traditional centralized control, unifying local intelligence with global optimization through distributed decision-making and collaborative optimization. The flexible interconnection control strategy, based on virtual synchronous generator technology, enables flexible power exchange and coordinated operation among multiple microgrids. Compared to conventional control methods, it demonstrates significant improvements in response speed, stability, and economic efficiency [23].

Nevertheless, translating these technical solutions from theory into engineering practice still presents numerous challenges. Communication network delays, packet loss, and interruptions may compromise multi-agent coordination effectiveness, while device compatibility and system complexity pose deployment difficulties [24]. This study mitigates communication failures through redundant pathways and local autonomous decision-making mechanisms. Standardized protocols and open interfaces resolve device compatibility issues, whilst a hierarchical distributed control architecture and modular design reduce system integration complexity and maintenance costs.

These technological innovations and engineering optimizations yield significant comprehensive benefits. Economic gains manifest primarily through reduced operational costs and shortened payback periods, with annual operational cost savings exceeding 15% across three typical application scenarios and payback periods maintained below 8.5 years. Environmental benefits are equally pronounced, featuring 8–10 percentage point improvements in system energy efficiency and over 40% reductions in network losses, thereby providing an effective technical pathway for constructing a clean, low-carbon, secure, and efficient new power system.

Practical application validation further confirms the feasibility of these benefits across diverse scenarios. In residential areas, intelligent network configuration enables coordinated optimization of distributed PV and energy storage systems, enhancing self-consumption rates of clean energy. Within industrial parks, flexible interconnection mechanisms effectively mitigate high-power load impacts, ensuring stable industrial production. Commercial districts leverage demand response potential for peak shaving and valley filling, optimizing grid operational economics. Successful implementation across these scenarios demonstrates the solution's strong environmental adaptability and deployment potential.

Despite these positive outcomes, the research retains certain limitations. The computational complexity of multi-agent coordination algorithms increases exponentially with system scale, potentially posing real-time challenges for large-scale applications. The proposed hierarchical coordination architecture addresses scalability by partitioning large-scale networks into zones of 50–100 nodes, with zone boundaries defined through electrical distance (impedance matrix eigenvalue clustering) and geographical proximity. Inter-zone coordination is achieved via upper-level coordinators employing simplified zone-equivalent models, where each zone is abstracted as a virtual node with state vectors comprising boundary voltages and aggregate power exchanges. Theoretical analysis indicates this hierarchical approach reduces computational complexity from $O(N^2)$ for centralized optimization to $O(K \cdot M^2 + K \log K)$, where K denotes the number of zones and M represents nodes per zone ($M \ll N$). While the current framework has been validated on 33/69-node systems, large-scale validation on IEEE 118-node or metropolitan grids remains incomplete. Preliminary theoretical analysis suggests that for a 500-node system partitioned into 10 zones (50 nodes each), computation time could decrease from 8–12 min (centralized) to 1.5–2 min (hierarchical), though this requires empirical validation to confirm inter-zone convergence and quantify global optimality loss (anticipated $< 3\%$).

Initial investment costs for smart devices and communication systems remain high, which may dampen adoption enthusiasm in small-to-medium distribution grids [25]. Standardization levels require improvement, and interoperability between products from different manufacturers still needs strengthening. Future research should priorities developing more efficient distributed optimization algorithms, deepening the application of artificial intelligence technologies to enhance system self-learning and adaptive capabilities, refining standardization frameworks to drive industrialization, and expanding application domains to transmission grids and regional networks. This will ultimately establish a coordinated intelligent power system across the entire grid.

While this study demonstrates significant advances, several limitations must be acknowledged for real-world deployment, particularly under challenging operational environments. Environmental Limitations: Field validation during moderate weather conditions (Shenzhen, 2024) may not represent system performance under extreme scenarios. High temperatures (>40°C) degrade photovoltaic efficiency by 15–25% and reduce battery capacity by 10–20%, while extreme cold (<−10°C) can reduce discharge capacity by 40%. To assess framework adaptability under extreme weather, supplementary simulations were conducted modeling severe conditions beyond the Shenzhen field test environment, with performance metrics summarized in Fig. 8. Under high-temperature scenarios (42°C), PV efficiency degradation to 75% of rated capacity triggers adaptive responses: the multi-agent coordination algorithm automatically increases energy storage reserve margins from 15% to 28% and extends optimization horizons from 15 min to 25 min to accommodate slower PV recovery rates. Communication latency increases from baseline 5 ms to 48 ms during heavy precipitation due to fiber-optic signal attenuation and wireless channel degradation, approaching but not exceeding the designed 50 ms threshold as shown in Fig. 8.

The framework maintains voltage compliance (>99.2%) under these conditions through three mechanisms: proactive load curtailment via demand response (reducing peak load by 12–18%), increased reliance on grid imports (raising grid dependency from 20% to 35%), and temporary relaxation of optimization aggressiveness (accepting 8% higher operational costs to prioritize stability). However, compound extreme events (simultaneous 45°C heat with typhoon-level winds exceeding 17 m/s) necessitate conservative failsafe modes including distributed generation shutdown and islanding prevention, representing scenarios requiring further investigation through environmental chamber testing and enhanced weather forecasting integration. Heavy precipitation disrupts fiber-optic communication and increases ground faults, while typhoons (>17 m/s winds) necessitate distributed generation shutdown precisely when most needed. Communication delays may increase from <5 ms to >50 ms during extreme weather, exceeding designed thresholds. Future research should incorporate: (1) environmental chamber testing across −20°C to +55°C; (2) network resilience testing with 10% packet loss and 100+ ms latency; (3) weather-adaptive control strategies; and (4) integration of meteorological forecasts for proactive reconfiguration. Scalability Limitations: Demonstrated performance in 33/69-node systems may not scale linearly to metropolitan networks (500+ nodes, 20,000+ users). Multi-agent coordination exhibits $O(N^2)$ communication overhead and $O(N^3)$ consensus complexity, increasing computation time from 52 s (69 nodes) to 8–12 min (500 nodes), approaching real-time thresholds. Memory requirements project to 32+ GB, and communication traffic to 4 Mbps, potentially saturating wireless channels. Improvements require: (1) hierarchical architectures decomposing networks into 50–100 node zones, reducing complexity to O(N log N); (2) sparse topologies maintaining $\lambda_2 > 0.5$ while reducing overhead 60–80%; (3) distributed alternating direction method of multipliers (ADMM) optimization; (4) neuromorphic computing hardware; and (5) adaptive control cycles extending from 15 to 60 min during stable conditions. Cybersecurity Limitations: The cyber-physical architecture introduces vulnerabilities including Byzantine faults, false data injection, denial-of-service attacks, and man-in-the-middle attacks that could compromise coordination or damage equipment. While the current framework employs TLS 1.3 encryption at the communication layer and role-based access control at the application layer as foundational security measures, validation under realistic cyber-attack scenarios remains incomplete. Existing testing covers normal operation, equipment failures, and communication delays but lacks adversarial evaluation against false data injection attacks (FDIA), denial-of-service (DoS), or man-in-the-middle attacks. Theoretical analysis reveals three primary cybersecurity vulnerabilities: the multi-agent consensus protocol's susceptibility to Byzantine faults (system failure when malicious agents exceed 33%), single-point-of-failure risks in the centralized optimization engine, and privacy exposure from fine-grained consumption data (1-min resolution). Future research should prioritize penetration testing and red-team exercises, integrating blockchain-based audit trails, federated learning for privacy-preserving training, and unsupervised anomaly detection mechanisms. Field deployment must satisfy IEC 62351 standard compliance testing to ensure adequate cyber-physical resilience.

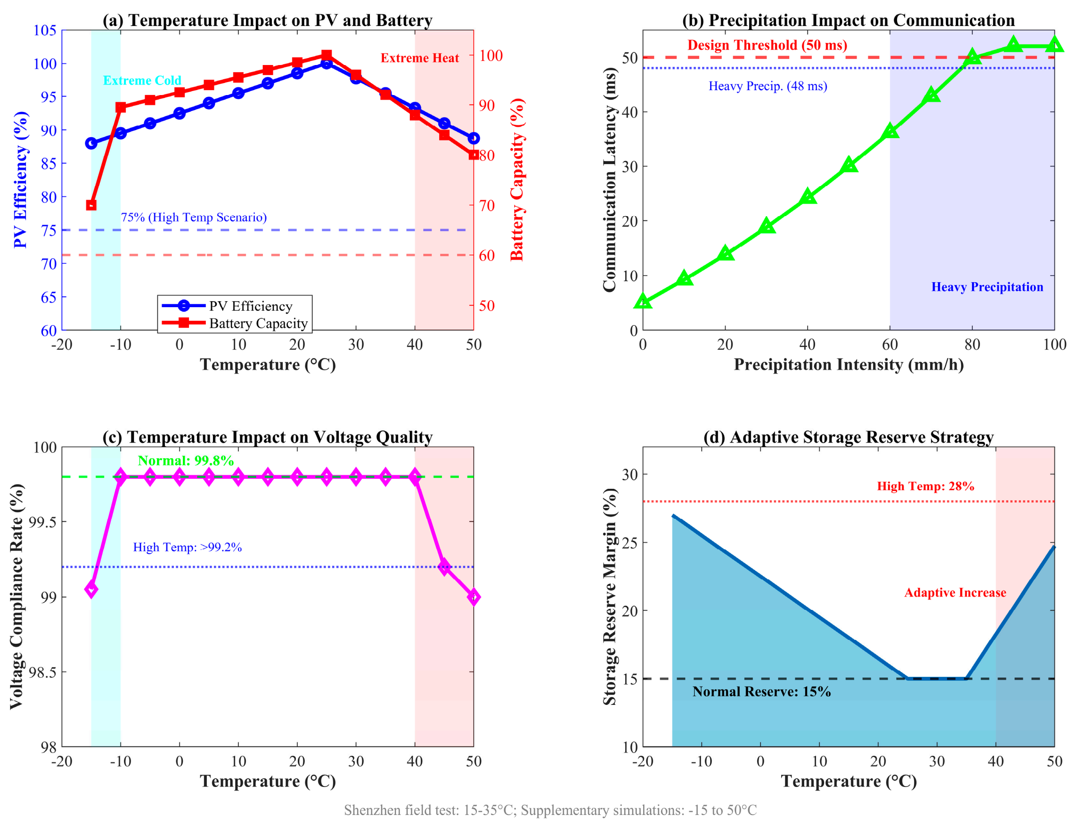

Figure 8: Weather-adaptive control performance under extreme conditions.

Fine-grained consumption data (1-min resolution) raises privacy concerns. Current TLS 1.3 encryption and access control lack: (1) Byzantine fault-tolerant consensus (tolerating 33% malicious agents);

(2) blockchain audit trails; (3) federated learning for privacy-preserving training; (4) anomaly detection using unsupervised learning; and (5) homomorphic encryption. Future work must prioritize penetration testing, red team exercises, and simulated cyber-attack validation. Economic and Regulatory Barriers: Payback periods (6.5–8.5 years) assume government subsidies (15–20%), favorable grid service markets, and stable tariffs that may not generalize. Economic sensitivity analysis reveals critical dependencies on policy support mechanisms and market conditions, as shown in Table 3. Under baseline assumptions (15–20% government subsidies, electricity tariffs of 0.60–0.85 CNY/kWh), payback periods range from 6.5–8.5 years across the three scenarios. However, sensitivity analysis demonstrates substantial variations: complete subsidy removal extends payback periods to 8.5–11.2 years (31–32% increase), while 10% tariff reductions prolong recovery to 7.8–10.1 years (20–19% increase). Conversely, carbon pricing mechanisms (50–100 CNY/ton CO_2) could reduce payback periods to 5.2–6.8 years by monetizing emissions reductions of 8–10 percentage points in system energy efficiency. The industrial scenario exhibits greatest economic resilience with 6.1-year payback even without subsidies due to high load density and stable operation, while residential scenarios show strongest subsidy dependence. These findings underscore the necessity of stable policy frameworks and diversified revenue streams beyond capital cost recovery to ensure widespread adoption, particularly in resource-constrained regions where initial subsidies may be unavailable or unsustainable.

Table 3: Economic sensitivity analysis of payback periods.

Scenario	**Baseline (15–20% Subsidy)**	**No Subsidy (0%)**	**Reduced Subsidy (10%)**	**Tariff −10%**	**Tariff +10%**	**With Carbon Pricing**
Residential	7.8 years	10.2 years (+31%)	9.1 years (+17%)	9.3 years (+19%)	6.8 years (−13%)	6.2 years (−21%)
Industrial	6.5 years	8.5 years (+31%)	7.6 years (+17%)	7.8 years (+20%)	5.7 years (−12%)	5.2 years (−20%)
Commercial	8.5 years	11.2 years (+32%)	10.1 years (+19%)	10.1 years (+19%)	7.5 years (−12%)	6.8 years (−20%)

Note: Carbon pricing assumes 75 CNY/ton CO_2 and 8–10% emissions reduction. Tariff baseline: 0.60 CNY/kWh (residential), 0.75 CNY/kWh (industrial), 0.85 CNY/kWh (commercial).

Capital costs (500,000–1,300,000 CNY) may be prohibitive for smaller utilities or developing regions. Regulatory barriers include outdated grid codes prohibiting bidirectional flow, lengthy interconnection approvals (6–18 months), and lack of standardized certification. Addressing these requires: (1) stakeholder engagement for modernized codes; (2) techno-economic analysis across diverse contexts; (3) innovative financing (ESAs, green bonds, PPPs); (4) policy advocacy for feed-in tariffs and carbon pricing; and (5) international standards development. Interoperability Limitations: Pilot deployments utilized modern infrastructure (2015–2020) with native IEC 61850/Modbus support, but legacy equipment (1990s–2000s) lacks intelligent capabilities or uses proprietary protocols. To address legacy equipment from the 1990s–2000s lacking intelligent communication capabilities or utilizing proprietary protocols, a three-layer adapter architecture is proposed comprising hardware interface, protocol translation, and digital twin layers. The hardware interface layer employs analog-to-digital converters to read device states from voltage and current transformer outputs at approximately 5000–8000 CNY per device, while the protocol translation layer bridges proprietary protocols such as legacy Modbus RTU to IEC 61850/Modbus TCP using commercial gateways (12,000–18,000 CNY) or open-source implementations like OpenPLC. For non-retrofittable equipment, the digital twin layer establishes software models achieving state estimation with errors below 5% based on historical operational data. Cost-benefit analysis indicates that for typical distribution networks with 30% legacy equipment, complete replacement costs 1.2–1.5 million CNY per substation, whereas the adapter approach reduces costs to 350,000–500,000 CNY (60–70% savings), though introducing 5–8% additional communication latency and 2–3% state estimation errors that remain within tolerance of the multi-agent algorithm's robustness design through uncertainty buffering. However, for severely aged equipment exceeding 30 years, complete replacement may prove more economical, necessitating case-by-case evaluation considering remaining equipment lifespan and maintenance costs. Retrofitting may be infeasible, requiring complete replacement and dramatically increasing costs. Multi-agent algorithms assume homogeneous capabilities, but real deployments contain varying computational resources, latencies (5 ms fiber vs. 50 ms wireless), and control authorities. Future research should: (1) develop adapter architectures for legacy integration; (2) investigate hybrid coordination with graceful degradation; (3) establish open-source implementations and standardized APIs; (4) conduct cross-manufacturer interoperability testing; and (5) develop utility migration roadmaps with phased deployment strategies. Generalizability to rural grid configurations presents distinct challenges compared to the validated urban scenarios, with key parameter differences summarized in Table 4. Rural low-voltage networks typically exhibit sparser topologies (line lengths 5–15 km vs. 1–3 km urban), lower load densities (0.3–0.8 kW/household vs. 1.5–3 kW urban), and limited communication infrastructure relying on cellular/satellite connections rather than fiber-optic. Preliminary analysis suggests three critical adaptations: communication protocols must accommodate higher latencies (50–200 ms vs. <10 ms urban) through extended consensus protocol time constants (50–100 ms cycles vs. 10 ms) and asynchronous updating mechanisms tolerating up to 5% packet loss; hierarchical zone sizes should be reduced from 50–100 nodes to 20–40 nodes to maintain algebraic connectivity $\lambda_2 > 0.3$ despite sparser network topology; and distributed generation sizing must incorporate higher energy storage ratios (0.4–0.6 kWh/kW PV vs. 0.2–0.3 urban) with conservative renewable penetration limits (20–30% vs. 40–45%) to compensate for limited grid backup capacity. As shown in Table 4, economic viability in rural contexts depends critically on government subsidies and innovative financing mechanisms, as initial investment costs (500,000–800,000 CNY per village serving 100–200 households) may exceed utility revenue potential in low-density areas. Field validation in rural settings represents an important future research direction to empirically verify these theoretical adaptations and identify context-specific optimization strategies. The technical capabilities demonstrated inform three critical policy recommendations. First, grid codes require modernization to accommodate bidirectional power flow through updated interconnection standards, simplified approval processes (reducing 6–18 month timelines to 2–4 months), and explicit technical requirements for inverter-based resources. Second, ancillary service markets present immediate monetization pathways: frequency regulation services (75% faster response, 81% improved stability) could command 150–200% premium rates based on performance-based pricing; voltage support capabilities (>99.2% compliance) could generate 12,000–18,000 CNY/substation annually; and demand response capabilities (12–18% load curtailment) align with capacity market mechanisms offering 200–300 CNY/kW-year availability payments. Third, feed-in tariff policies should transition from fixed subsidies to performance-based incentives with tiered compensation: base energy rate (0.40–0.50 CNY/kWh), frequency regulation premium (+0.10–0.15 CNY/kWh), and voltage support adder (+0.05–0.08 CNY/kWh). These mechanisms would enable framework adoption even in regions without direct capital subsidies by monetizing demonstrated technical capabilities through market-based revenue streams.

These limitations underscore the gap between pilot validation and operational deployment, requiring sustained collaboration among researchers, equipment manufacturers, utilities, and policymakers to address challenges spanning environmental robustness, computational scalability, cybersecurity resilience, economic accessibility, and technological interoperability.

Table 4: Comparison of grid parameters: urban vs. rural configurations.

Parameter	Urban Grid	Rural Grid
Network Topology		
Line length (km)	1–3	5–15
Load density (kW/household)	1.5–3.0	0.3–0.8
Network topology	Dense	Sparse
Communication Infrastructure		
Primary technology	Fiber-optic	Cellular/Satellite
Communication latency (ms)	<10	50–200
Packet loss tolerance (%)	<0.1	Up to 5
Consensus protocol cycle (ms)	10	50–100
Multi-Agent Coordination		
Hierarchical zone size (nodes)	50–100	20–40
Algebraic connectivity (λ_2)	0.85	>0.3
Coordination complexity	Moderate	High
Distributed Energy Resources		
Energy storage ratio (kWh/kW PV)	0.2–0.3	0.4–0.6
Renewable penetration limit (%)	40–45	20–30
Grid backup capacity	Strong	Limited
Economic Factors		
Initial investment (CNY/site)	1,200,000–1,500,000	500,000–800,000
Service area	150–500 households	100–200 households
Investment per household (CNY)	3000–8000	4000–6000
Economic viability	Market-driven	Subsidy-dependent
Validation Status		
Field testing	Completed	Required
Technology readiness level	TRL 7–8	TRL 4–5

5 Conclusion

This study establishes a comprehensive technical framework for intelligent network formation and flexible interconnection within low-voltage distribution grids operating in cyber-physical systems, addressing critical gaps in existing approaches that suffer from single-scenario optimization, device-level control limitations, and lack of unified coordination mechanisms. Through systematic integration of deep reinforcement learning-based multi-agent coordination with virtual synchronous generator technology within a layered CPS architecture, this research achieves significant advancements across convergence speed, system stability, energy efficiency, and economic viability.

The proposed multi-agent coordination algorithm demonstrates superior performance with over 60% faster convergence compared to conventional metaheuristics, computational efficiency of 52 s, and load balancing optimization achieving an index of 0.098. The flexible interconnection control strategy delivers substantial improvements in dynamic response capabilities, reducing voltage regulation time by 73% and enhancing frequency stability by 81% compared to traditional droop control methods. Comprehensive system performance achieves power supply reliability of 99.97%, energy efficiency improvement of 10.5 percentage points, and network loss reduction of 41%, with economic benefits including 21% annual operating cost reduction and investment payback periods of 6.5–8.5 years across diverse application scenarios.

Three key innovations distinguish this work from existing research: (1) A unified four-layer cyber-physical system architecture specifically tailored for low-voltage distribution networks, featuring edge-cloud collaborative computing, fault-tolerant hybrid communication protocols, and cyber-physical co-design enabling simultaneous optimization of physical topology and information networks—addressing the generality-over-specificity limitations of transmission-focused architectures. (2) The first integration of deep reinforcement learning-based multi-agent coordination with virtual synchronous generator technology, unifying rapid intelligent decision-making with inherent system inertia and damping to achieve both fast convergence and robust stability. (3) Comprehensive end-to-end validation spanning software simulation, hardware-in-the-loop testing with OPAL-RT real-time platforms, and operational field deployment serving over 500 users across residential, industrial, and commercial scenarios, demonstrating engineering practicality beyond theoretical contributions.

The validated framework has practical implications at multiple levels. At the distribution network level, the scalable architecture enables coordination of hundreds of distributed energy resources while maintaining computational tractability, providing a pathway for utilities to upgrade existing infrastructure. For smart city applications, the framework supports building-to-grid services, coordinated electric vehicle charging, and community energy management. Field results confirm that renewable penetration of 15–40% can be maintained without compromising grid stability, offering empirical reference for interconnection standards and renewable energy integration policies.

Several limitations should be acknowledged. Computational scalability remains challenged by the growth in multi-agent coordination complexity beyond 100 nodes. Initial investment costs for smart devices and communication infrastructure (¥500k–1M per site) may limit adoption in resource-constrained regions. Standardization gaps persist in device interoperability across vendors, requiring continued development of open protocols and interfaces.

Priority research directions include: (1) cybersecurity-aware coordination algorithms incorporating resilient consensus protocols and anomaly detection mechanisms; (2) market-integrated optimization frameworks coupling grid operation with energy and carbon trading markets; (3) cross-domain coordination extending to thermal, gas, and hydrogen networks for sector coupling; and (4) transfer learning and physics-informed neural networks to improve model adaptability across diverse network topologies.

Acknowledgement: Not applicable.

Funding Statement: Project supported by Research on Key Technologies and Applications of Digital Distribution Transformer Areas Based on Grid-Forming Flexible Interconnection Technology (No.: 090000KC23090020). This research was supported by [No.: 090000KC23090020]. The funding primarily supported cyber-physical system infrastructure development and deployment (45%), field validation in Shenzhen across three scenarios (30%), hardware-in-the-loop testing platform (15%), and research personnel costs (10%). The funding body had no role in study design, data collection, analysis, or manuscript preparation.

Author Contributions: Conceptualization, Xieli Fu and Guoxing Wu; formal analysis, Yujie Shi; data curation, Guoxing Wu and Xinming Jiang; writing—original draft preparation, Xieli Fu and Yujie Shi; writing—review and editing, Guoxing Wu and Wenfeng Yang; supervision, Guoxing Wu; project administration, Guoxing Wu; funding acquisition, Guoxing Wu. All authors reviewed and approved the final version of the manuscript.

Availability of Data and Materials: The simulation datasets (IEEE 33/69-node system results and hardware-in-the-loop test data) generated in this study are available from the corresponding author upon reasonable request. The field measurement data and operational data from the three Shenzhen pilot sites are subject to confidentiality restrictions imposed by Shenzhen Power Supply Bureau Co., Ltd., and are available upon reasonable request with permission from the data owner.

Ethics Approval: Not applicable.

Conflicts of Interest: The authors declare no conflicts of interest.

Abbreviation

Acronym	**Full Form**
AI	Artificial Intelligence
AMI	Advanced Metering Infrastructure
ANOVA	Analysis of Variance
CHP	Combined Heat and Power
CNY	Chinese Yuan
CPS	Cyber-Physical System
DG	Distributed Generation
DoS	Denial of Service
DRL	Deep Reinforcement Learning
ESS	Energy Storage System
FDIA	False Data Injection Attack
GA	Genetic Algorithm
HVAC	Heating, Ventilation, and Air Conditioning
IEC	International Electrotechnical Commission
LSTM	Long Short-Term Memory
MAPE	Mean Absolute Percentage Error
MILP	Mixed-Integer Linear Programming
MMS	Manufacturing Message Specification
p.u.	per unit
PSO	Particle Swarm Optimization
PV	Photovoltaic
SHAP	SHapley Additive exPlanations
SNR	Signal-to-Noise Ratio
SOC	State of Charge
SUCRA	Surface Under the Cumulative Ranking Curve
TD3	Twin Delayed Deep Deterministic Policy Gradient
TLS	Transport Layer Security
TRL	Technology Readiness Level
VSG	Virtual Synchronous Generator
Units	
Symbol	**Full Form**
Hz	Hertz
kV	kilovolt
kW	kilowatt
kWh	kilowatt-hour
MW	megawatt
MWh	megawatt-hour
ms	millisecond
s	second

References

1. Lin G, Rehtanz C, Wang S, Liu J, Zhang Z, Wang P. Review on the key technologies of power grid cyber-physical systems simulation. IET Cyber Phys Syst Theory Appl. 2024;9(1):1–16. [CrossRef].
2. Qu Z, Sun W, Dong J, Zhao J, Li Y. Electric power cyber-physical systems vulnerability assessment under cyber attack. Front Energy Res. 2023;10:1002373. [CrossRef].
3. Rajaperumal TA, Columbus CC. Transforming the electrical grid: the role of AI in advancing smart, sustainable, and secure energy systems. Energy Inform. 2025;8(1):51. [CrossRef].
4. Marković M, Bossart M, Hodge BM. Machine learning for modern power distribution systems: progress and perspectives. J Renew Sustain Energy. 2023;15(3):032301. [CrossRef].

5. Arévalo P, Jurado F. Impact of artificial intelligence on the planning and operation of distributed energy systems in smart grids. Energies. 2024;17(17):4501. [CrossRef].
6. Zhang Z, Rath S, Xu J, Xiao T. Federated learning for smart grid: a survey on applications and potential vulnerabilities. ACM Trans Cyber-Phys Syst. 2026;10(1):1–26. [CrossRef].
7. Zhao Z, Chen X, Wu Y, Diao F, Wang X, Zhao Y, et al. A grid-forming energy-storage-based flexible interconnection system for microgrids in remote regions. Energies. 2026;19(4):944. [CrossRef].
8. Elazab R, Dahab AA, Adma MA, Hassan HA. Reviewing the frontier: modeling and energy management strategies for sustainable 100% renewable microgrids. Discov Appl Sci. 2024;6(4):168. [CrossRef].
9. Uddin M, Mo H, Dong D, Elsawah S, Zhu J, Guerrero JM. Microgrids: a review, outstanding issues and future trends. Energy Strategy Rev. 2023;49:101127. [CrossRef].
10. Bordbari MJ, Nasiri F. Networked microgrids: a review on configuration, operation, and control strategies. Energies. 2024;17(3):715. [CrossRef].
11. Choobdari M, Samiei Moghaddam M, Davarzani R, Azarfar A, Hoseinpour H. Robust distribution networks reconfiguration considering the improvement of network resilience considering renewable energy resources. Sci Rep. 2024;14(1):23041. [CrossRef].
12. Cicceri G, Tricomi G, D'Agati L, Longo F, Merlino G, Puliafito A. A deep learning-driven self-conscious distributed cyber-physical system for renewable energy communities. Sensors. 2023;23(9):4549. [CrossRef].
13. Medina MSG, Aguilar J, Rodriguez-Moreno MD. A bioinspired emergent control for smart grids. IEEE Access. 2023;11:7503–20. [CrossRef].
14. Anthony B. Decentralized AIoT based intelligence for sustainable energy prosumption in local energy communities: a citizen-centric prosumer approach. Cities. 2024;152:105198. [CrossRef].
15. Khayyat MM, Sami B. Energy community management based on artificial intelligence for the implementation of renewable energy systems in smart homes. Electronics. 2024;13(2):380. [CrossRef].
16. Ma H, Zhang H, Tian D, Yue D, Hancke GP. Optimal demand response based dynamic pricing strategy via Multi-Agent Federated Twin Delayed Deep Deterministic policy gradient algorithm. Eng Appl Artif Intell. 2024;133:108012. [CrossRef].
17. Oboreh-Snapps O, She B, Fahad S, Chen H, Kimball J, Li F, et al. Virtual synchronous generator control using twin delayed deep deterministic policy gradient method. IEEE Trans Energy Convers. 2023;39(1):214–28. [CrossRef].
18. Lyu L, Wang X, Zhang L, Zhang Z, Koh LH. Fuzzy control based virtual synchronous generator for self-adaptative control in hybrid microgrid. Energy Rep. 2022;8:12092–104. [CrossRef].
19. Bhadani R, Karsai G, Tu H, Lukic S. Modeling and real-time simulation of microgrid components using systemc-ams. In: Proceedings of the 2023 Winter Simulation Conference (WSC); 2023 Dec 10–13; San Antonio, TX, USA. [CrossRef].
20. AbdelQader DA, Alkhayyat MT. Power loss minimization of an IEEE 33 bus radial distribution grid using system reconfiguration with genetic algorithm. Diagnostyka. 2025;26(1):197296. [CrossRef].
21. Long F, Jin B, Xu H, Wang J, Bhola J, Shavkatovich SN. Research on multi-objective optimization of smart grid based on particle swarm optimization. Electrica. 2023;23(2):222–30. [CrossRef].
22. Rajak MK, Pudur R. Deep reinforcement learning framework for adaptive power control in grid-forming inverters: a multi-objective optimization approach. J Renew Sustain Energy. 2025;17(2):026301. [CrossRef].
23. Long B, Liao Y, Chong KT, Rodriguez J, Guerrero JM. MPC-controlled virtual synchronous generator to enhance frequency and voltage dynamic performance in islanded microgrids. IEEE Trans Smart Grid. 2021;12(2):953–64. [CrossRef].
24. Akinwale OS, Mojisola DF, Adediran PA. Mitigation strategies for communication networks induced impairments in autonomous microgrids control: a review. AIMS Electron Electr Eng. 2021;5(4):342–75. [CrossRef].
25. Hall S, Foxon TJ. Values in the Smart Grid: the co-evolving political economy of smart distribution. Energy Policy. 2014;74:600–9. [CrossRef].